Preliminary Change Request for the SNS Ring Hybrid Lattice

BNL/SNS TECHNICAL NOTE

NO. 066

J. Wei, editor

October 12, 1999

COLLIDER ACCELERATOR DEPARTMENT
BROOKHAVEN NATIONAL LABORATORY
UPTON, NEW YORK 11973

Preliminary Change Request for the SNS Ring Hybrid Lattice

(October 12, 1999)

Preface

Since the Accelerator System Advisory Committee review of the Spallation Neutron Source (SNS) Project [1] on October 1998, the physics and engineering groups at the Brookhaven National Laboratory have been studying on improving the machine lattice and the design performance of the SNS accumulator ring [2, 3]. The main goals of the study are to improve the maintainability and flexibility of the machine, and to reduce uncontrolled beam loss and activation. Since the SNS project was approved for construction on October 1998, every effort is made to minimize the impact on project cost and schedule.

This report documents study results based on which a change request was made for the SNS ring lattice. On October 1999, the change request was presented to the SNS management and a review committee consisting of A. Chao, Y. Cho, D. Finley, M. Harrison, R. Kustom, D. Lowenstein, R. Macek, and E. Temple. The committee endorsed the change request.

Contents

1 Overview

1.1 Introduction

The Spallation Neutron Source (SNS) is designed to meet the growing need for new tools that will deepen our understanding in materials science, life science, chemistry, fundamental and nuclear physics, earth and environmental sciences, and engineering sciences. The SNS is based on an accelerator producing an average beam power of 2 MW at a repetition rate of 60 Hz. The accelerator complex [1] consists of the source and the front end, a 1 GeV full-energy Linac, a single accumulator ring and its transfer lines, and the target. This report documents the optimization study of the accumulator ring lattice design.

1.2 Design Philosophy

Reliability and maintainability are of primary importance to the SNS facility. Based on operational experience at Linac [4], AGS, and AGS Booster [5], hands-on maintenance demands that the average uncontrolled beam loss be limited to about 1 to 2 W of beam power per tunnel meter. For the accumulator ring with a circumference of 220 meters, this corresponds to an average uncontrolled beam loss of about 10^{-4} at 1 GeV beam energy.

Among the existing proton synchrotrons and accumulator rings, the lowest achievable beam loss is about 3×10^{-3} at the Proton Storage Ring at the Las Alamos National Laboratory. These beam losses are typically attributed to a high space change tune shift (0.25 or larger), limited physical and momentum acceptance, injection loss (especially for H^- injection), large magnet errors (especially for rapid cycling synchrotrons), and instabilities (e.g. PSR instability).

The SNS ring is designed with practically achievable large acceptance so that beam space charge tune shift is below 0.2. The transverse acceptance-to-emittance ratio is about 3, and the momentum aperture is $\pm2\%$ in $\Delta p/p$. The injection layout and magnet field is carefully designed to prevent pre-mature H^- and H^0 stripping. Main magnet field is kept moderate to avoid saturation, and pole tip shimming is performed on both dipole and quadrupole magnets to compensate fringe field contribution. Finally, vacuum chamber is coated, chamber steps are tapered, and injection beam momentum is broadened to avoid instabilities [6, 13].

Effective collection of the beam halo is essential for maintaining a low uncontrolled beam loss [7, 8, 9]. To facilitate the momentum cleaning and multi-stage collimation systems, a wide momentum acceptance (full beam plus $\pm2\%$ in $\Delta p/p$) is essential. This allows cleaning of the momentum halo using a multi-turn beam gap kicker system [10]. With the collimation system designed to be more than 90% efficient, the total allowed beam loss at collimators [11] is at 10^{-3} level.

Flexibility is another important aspect considered in the design. A matched FODO/doublet hybrid lattice [2] is chosen so that chromatic and resonance correction can be done mainly in the FODO arcs, while long uninterrupted doublet straight sections allow flexible arrangement of injection modules that is independent of lattice tuning, and flexible placement of collimators for phase space collimation optimization. Since the FODO arc and doublet straight section are optically matched, a low amplitude (β_{max}) is achieved for the given cell length, thus confining

the beam size.

To address the issue of engineering reliability [12], the collimator and shielding hardware are designed to withstand an average of 10^{-2} beam power. In addition, the machine is designed to withstand a couple of full beam pulses during commissioning and in case of emergency.

Since the SNS project has already been in construction since October 1998, every effort is made to minimize the impact of lattice change on project cost and schedule. The foot-print of the ring is kept unchanged, and the ring dipole and regular quadrupole specification remain the same. On the other hand, with the lattice change the ring acceptance is increased by more than 50%, and the long uninterrupted straight section is increased from 5.2 m (4 sections per period) to 9.0 m (plus two 5.5 m section for each period).

1.3 Acknowledgments

Contributors:

D. Abell, J. Beebe-Wang, M. Blaskiewicz, J. Brodowski, P. Cameron, N. Catalan-Lasheras, A. Fedotov, C. Gardner, H.C. Hseuh, Y.Y. Lee, N. Malitsky, D. Raparia, J. Sandberg, N. Tsoupas, J. Tuozzolo, J. Wei, W.T. Weng, S. Y. Zhang

Acknowledgments:

J. Alessi, G. Danby, J.D. Galambos, R.L. Gluckstern, J. Jackson, D. Kaltchev, R. Kustom, J.B. Jeanneret, D. Lowenstein, A.U. Luccio, H. Ludewig, W. Meng, J-L. Mi, J. Negrin, M. Nekulak, C-I. Pai, K. Reece, T. Roser, H. Schonauer, A. Soukas, R. Talman, S. Tepikian, D. Trbojevic, R. Witkover, A. Zaltsman, and the SNS team at the Brookhaven National Laboratory.

Special Acknowledgments:

Y. Cho, S. Machida, G. Rees

Editor:

J. Wei

2 Justification

The Spallation Neutron Source is based on an accelerator producing an average beam power of 2 MW at a repetition rate of 60 Hz. The accelerator complex consists of an ion source and a front end, a Linac, and an accumulator ring and its transfer lines. The proposed change request is on the ring and its transfer lines, proposing to change the ring lattice from all-FODO to hybrid lattice in the so-called omega configuration.

2.1 Original Design

As shown in Figure 1, the original SNS ring is designed in a so called alpha configuration where the HEBT and RTBT transfer lines cross each other with a vertical separation. The

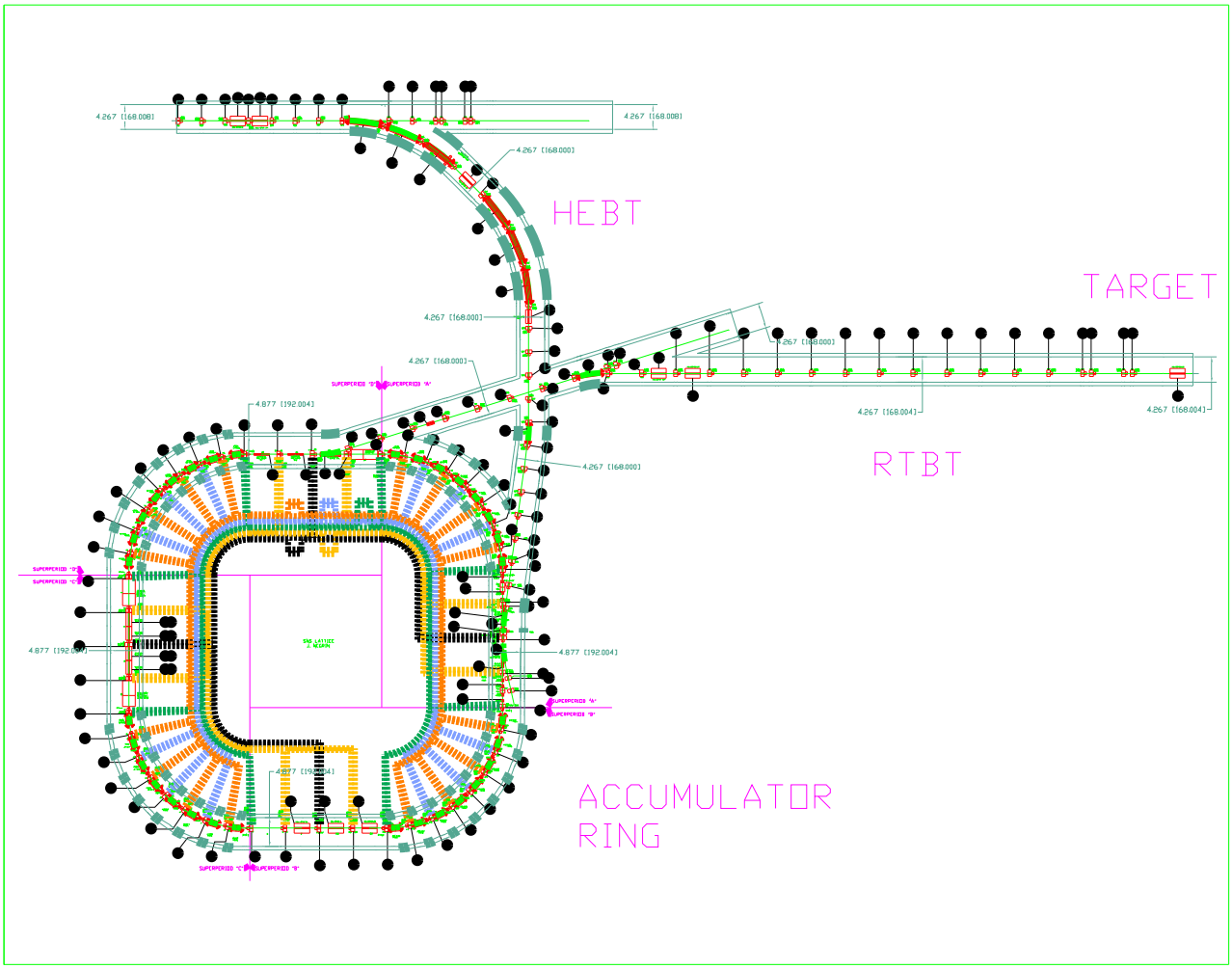

Figure 1: Layout of the original all-FODO lattice in the alpha configuration for the Spallation Neutron Source ring.

ring lattice is four-fold symmetric with each super-period containing one FODO arc section and one FODO straight section. The arc section consists of four 8-meter long FODO cells, each with a horizontal betatron phase advance of 90 degrees. The dispersion-free straight section consists of two 11.58-meter long FODO cells. The available uninterrupted drift space is about 5.2 meters.

The ring has 32 arc dipole magnets and 48 quadrupole magnets. The inscribed diameters are 31 cm for the 8 quadrupoles located in the middle of the straight sections and the middle of the arcs, and 21 cm for the other 40 quadrupoles.

As shown in Figure 2, the acceptance of the ring is about 306 πmm·mr in the transverse directions for particles of relative momentum deviation up to $\pm 0.7\%$. In order to reach a space charge tune shift of about 0.2, the beam is painted to an emittance of 120 πmm·mr in both the horizontal and vertical directions. However, since the painting is performed using the correlated method, the maximum total transverse emittance is 240 πmm·mr. We choose the

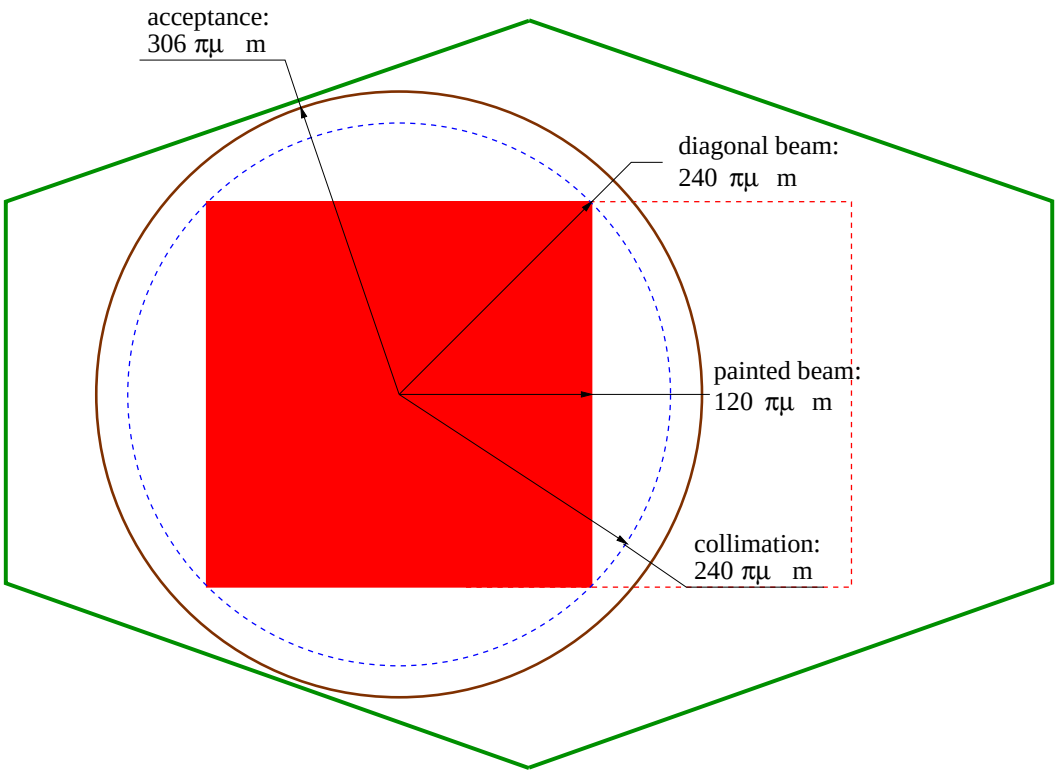

Figure 2: Schematic illustration of the beam emittance, collimation admittance, and vacuum chamber acceptance of the original all-FODO SNS ring. The green octagonal box indicates the vacuum chamber cross section (23 cm width, 15.2 cm height). The red squares correspond to off-momentum at $\Delta p/p$ of $\pm 0.7\%$. The ring magnet acceptance is 306 πmm·mr for $\pm 0.7\%$ off-momentum beam, and 360 πmm·mr for on-momentum beam. The total transverse emittance is up to 240 πmm·mr. Ring collimation is planned at 240 πmm·mr.

acceptance of the ring collimation system to be about 240 πmm·mr. As shown in Figure 3, with compensated magnetic field errors and corrected misalignments, the beam fraction collected by the collimation system is about 2%. Figure 4 shows expected collimation efficiency as a

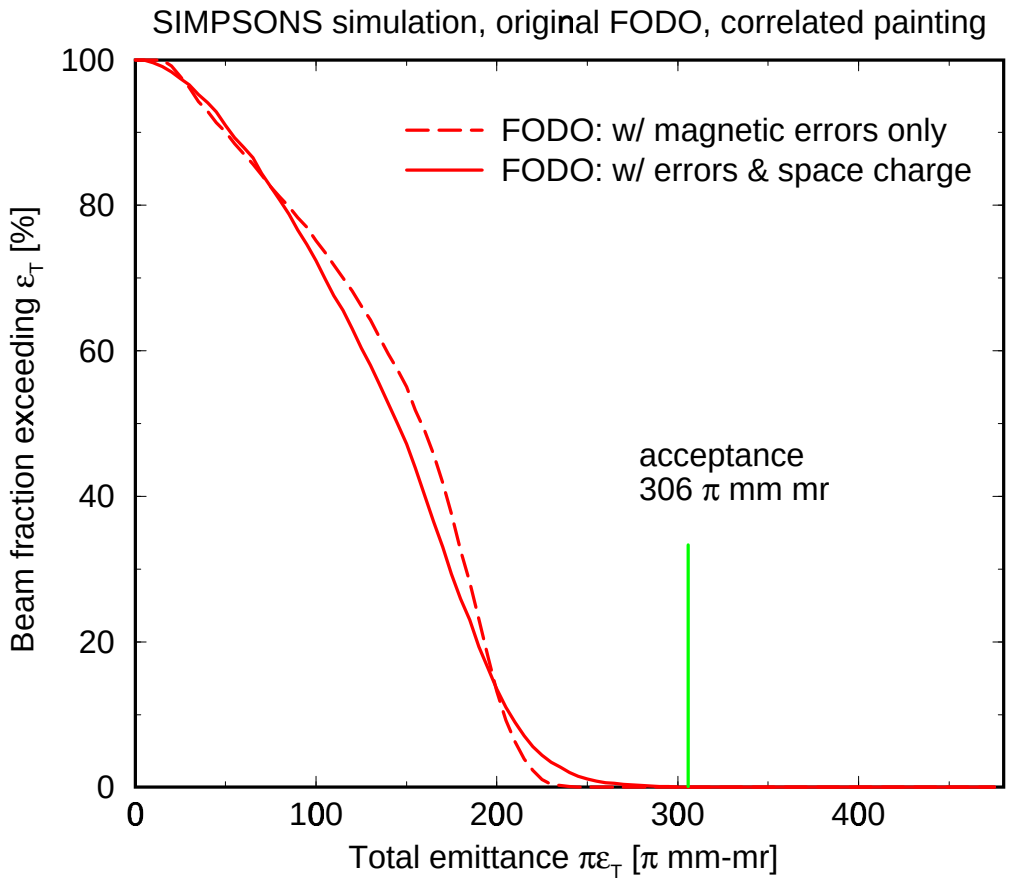

Figure 3: Fraction of the beam exceeding a given total transverse emittance at the end of injection painting. The simulation is performed with the SIMPSONS program incorporating space charge, magnetic errors, and misalignments. The beam exceeding the planned primary collimation at 240 πmm·mr is about 2%.

function of the available ring acceptance. We track particles around the ring using a diffusion model where particles drift slowly outwards from the beam core into the collimation system. Computer program K2 is used to perform Monte-carlo simulation of nuclear and Coulomb scattering of the collimator surface. After the first passage of the particle through the system, their amplitude is recorded. The collimation inefficiency is then defined as the relative number of halo particles escaping the system above the ring acceptance. At a design vacuum chamber acceptance of 306 πmm·mr, the expected collimation efficiency is about 80% when the primary collimation is performed at 240 πmm·mr. The expected uncontrolled beam loss is at 10^{-3} level.

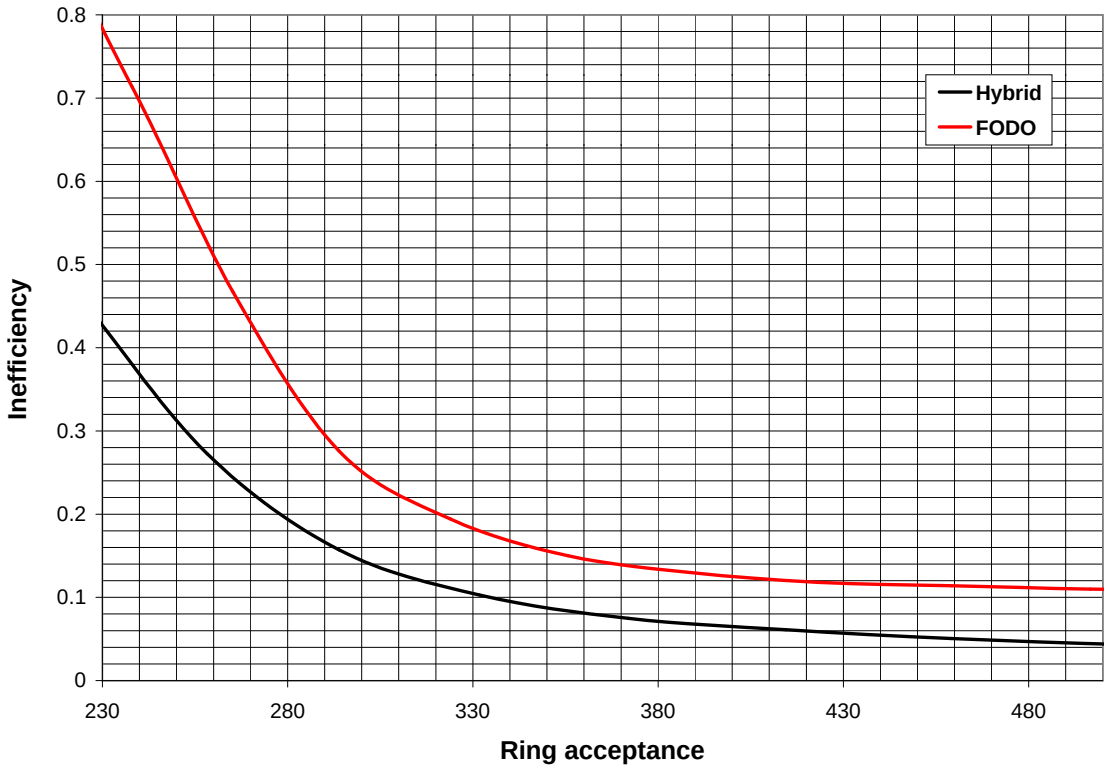

Figure 4: Comparison of collimation efficiency between the original all-FODO lattice (top curve) and the proposed hybrid lattice (bottom curve). The inefficiency is defined as the number of halo particles escaping the collimation system after one turn above a given amplitude. The efficiency corresponding to the original design acceptance of 306 πmm·mr is below 80%.

2.2 Proposed Design

As shown in Figure 5 for the proposed omega configuration, the HEBT and RTBT transfer lines no longer cross each other, thus simplifying operation and maintenance [13]. The ring lattice is four-fold symmetric with each super-period containing one FODO arc section and one doublet straight section. The arc section consists of four 8-meter long FODO cells, each with a horizontal betatron phase advance of 90 degrees. The dispersion-free straight section consists of one 9.04-meter and two 5.45-meter uninterrupted drift spaces.

The ring has 32 arc dipole magnets and 52 quadrupole magnets. The inscribed diameters are 26 cm for the 24 quadrupoles located in the straight sections and the high-dispersion locations of the arcs, and 21 cm for the other 28 quadrupoles.

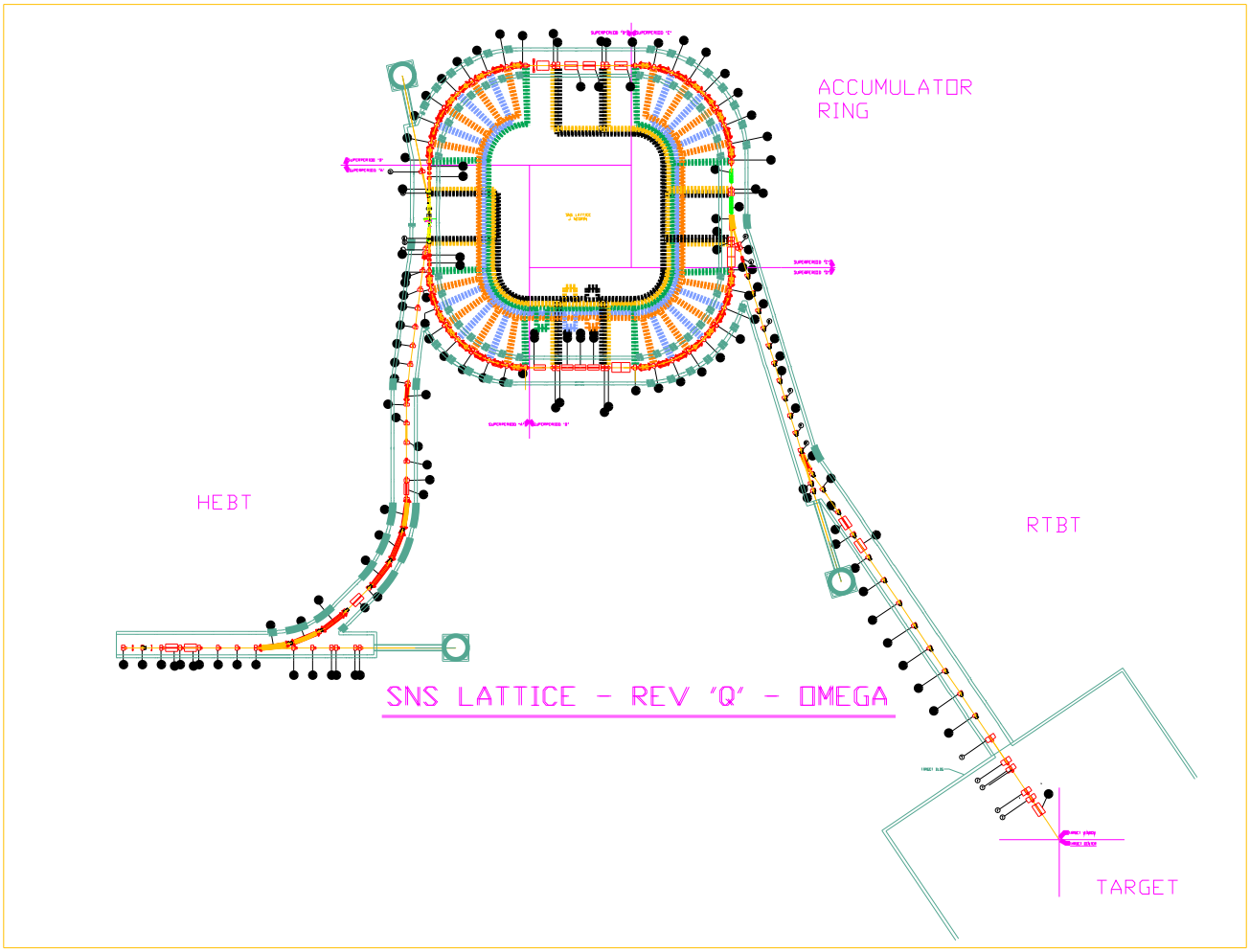

Figure 5: Layout of the proposed FODO-doublet hybrid lattice in the omega configuration for the Spallation Neutron Source ring.

2.2.1 Layout and space

Figure 6 shows the schematic layout of the ring. The four straight sections are mainly designed for beam injection, beam collimation, extraction, and RF systems. Figure 7 shows the layout of the lattice magnets (dipole, quadrupole, sextupole, and correctors) in one of the four lattice super-periods. Dipole correctors in both the arc and straight sections are used for misalignment closed orbit correction. The sextupoles in the arc sections are used for chromaticity adjustment, off-momentum optics matching, and momentum aperture improvement. The multi-layer correctors in the straight sections are used for resonance corrections.

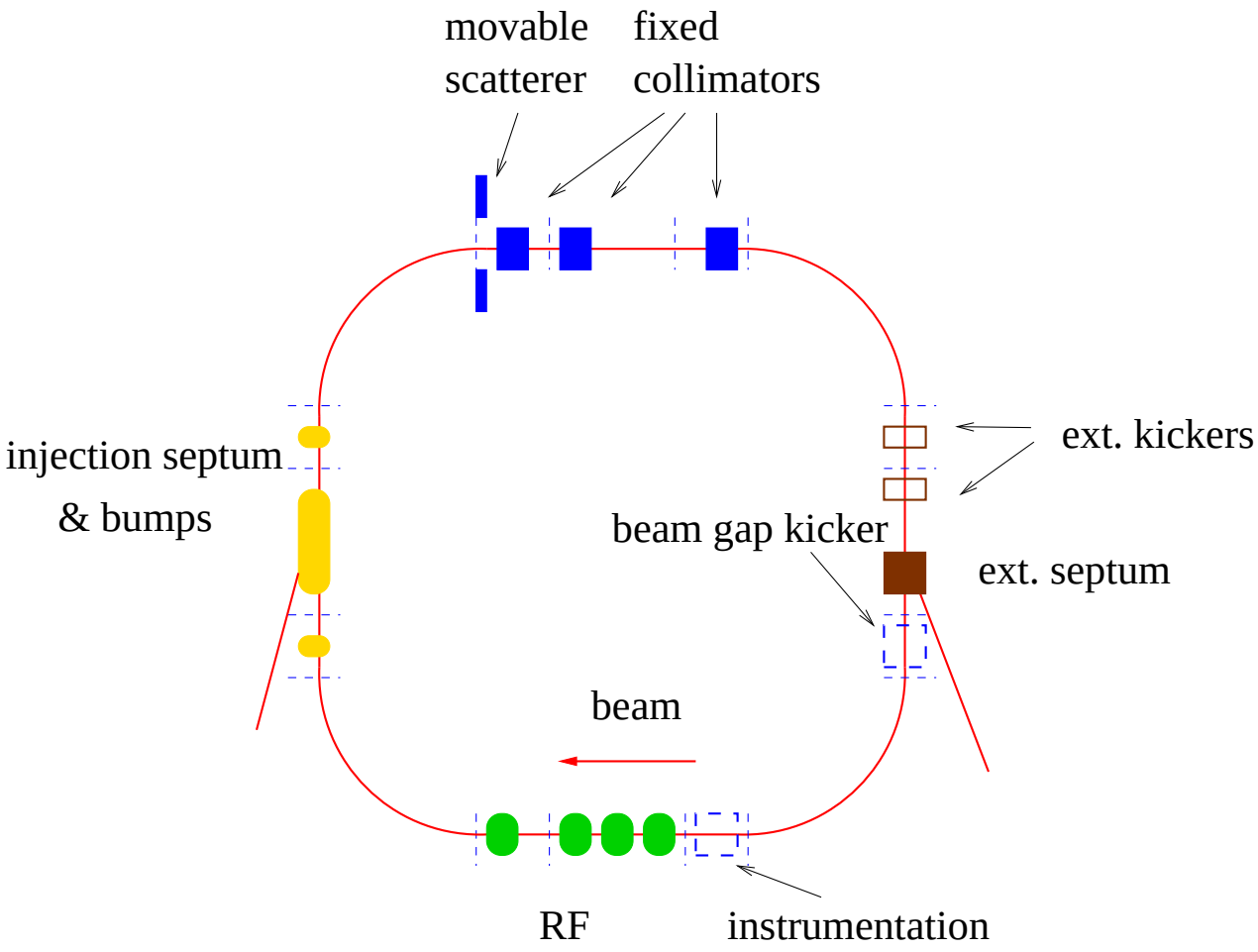

Figure 6: Schematic layout of the proposed SNS ring in the omega configuration.

Each of the 4 lattice period contains a straight section that has one 9.04 m and two 5.50 m drift spaces. The total straight section length is about 80 meters. For each drift space, the "overhead" taken by correctors, BPMs, vacuum pumps, bellows, flanges, etc. is about 1.5 meters. The total usable length is about 62 meters. Each period has 4 m – 7.5 m – 4 m structure. The total unclaimed dispersion-free drift space is about 14 meters, among which 8 meters are located in the collimation section. For the arc section, the layout is mirror-symmetric with respect to the middle of the arc to minimize vacuum chamber type.

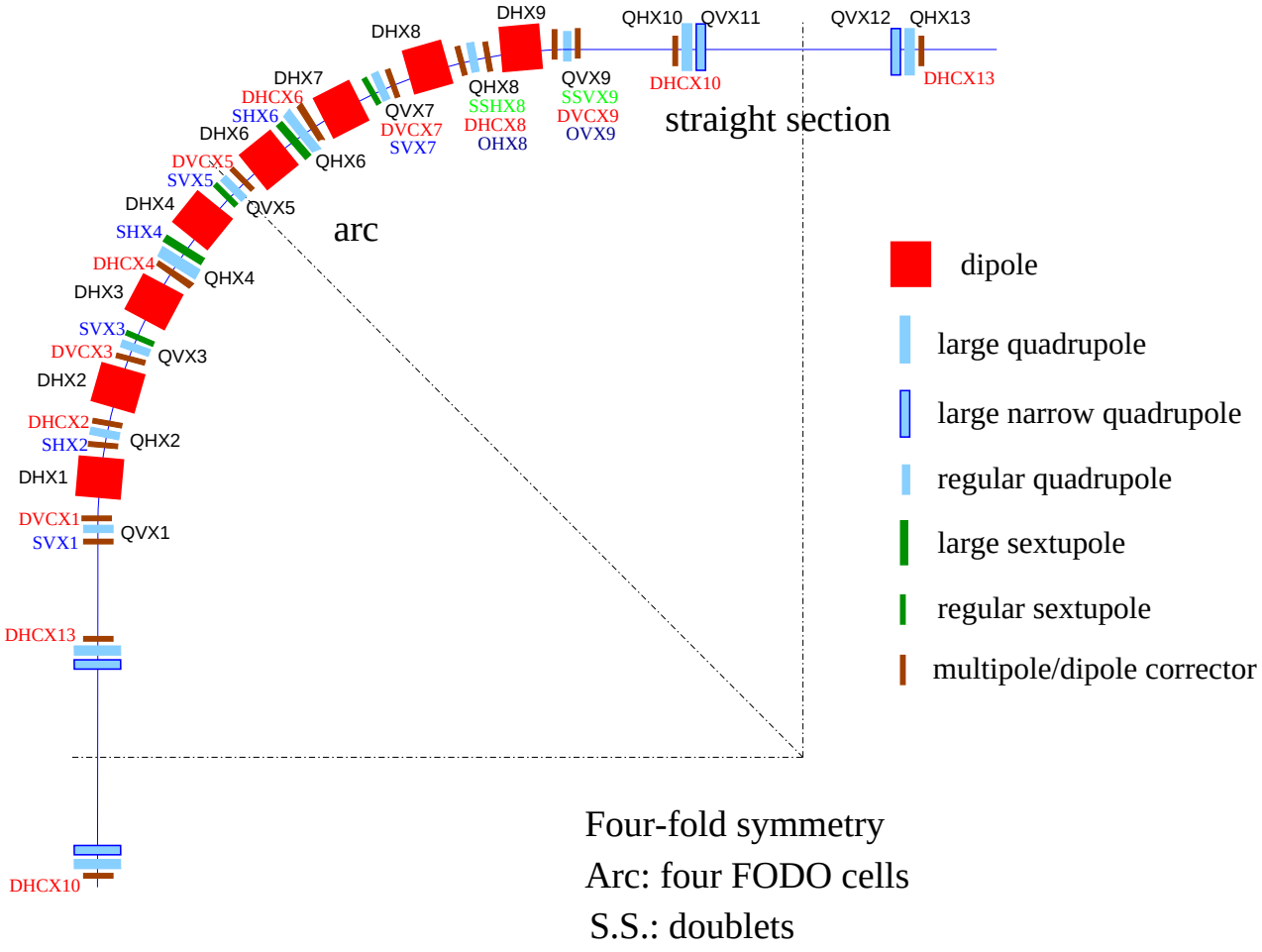

Figure 7: Schematic layout showing dipole, quadrupole, sextupole, and corrector magnets of one lattice super-period.

2.2.2 Parameters

Table 1 lists major machine and beam parameters for the proposed hybrid lattice ring. The nominal working point in the transverse tune space (Q_x, Q_y) is (6.30, 5.80), with the horizontal and vertical tunes split by half a unit. The lattice is tunable over a range of more than one unit. Three alternative working points are (6.30, 5.27), (5.82, 4.80) and (5.82, 5.80). Table 2 summarizes the evolution of beam parameters from Linac to the ring with anti-correlated or coupled injection painting. The final transverse beam distribution is quasi-uniform in a elliptical area satisfying the required current density limit of below 0.25 A/m^2.

Table 1: Major machine parameters for the proposed hybrid lattice Spallation Neutron Source ring.

Quantity	Value	unit
Circumference	220.88	m
Average radius	35.154	m
Injection energy	1	GeV
Extraction energy	1	GeV
Beam power	2	MW
Repetition rate per ring	60	Hz
Number of proton	2.08	10^{14}
Ring dipole field	0.7406	T
RF harmonic	1, 2	
Peak RF voltage, $h = 1$	40	kV
Peak RF voltage, $h = 2$	20	kV
Normalized emittance	289	π mm mr
Unnormalized emittance (99%)	160	π mm mr
Betatron acceptance	480	π mm mr
Momentum acceptance (full beam)	$\pm$ 2	%
Momentum acceptance (zero amplitude)	$\pm$ 3.8	%
Magnetic rigidity, $B\rho$	5.6575	Tm
Bending radius, ρ	7.6394	m
Horizontal tune	5.8 – 6.8	
Vertical tune	4.8 – 5.8	
Transition energy, γ_T	4.95	
Horizontal natural chromaticity	-7.5	
Vertical natural chromaticity	-6.3	
Number of super-period	4	
Arc lattice	4 FODO cells	
Arc cell length	8	m
Straight section lattice	2 doublets	
Straight section drift length	9.04, 2×5.45	m

2.2.3 Acceptance and momentum aperture

The acceptance of the ring is 480 πmm·mr in the transverse directions for particles of relative momentum deviation up to $\pm 1\%$. The injection area is designed to accommodate both anti-correlated and correlated painting schemes, as shown in Figure 8. With anti-correlated or

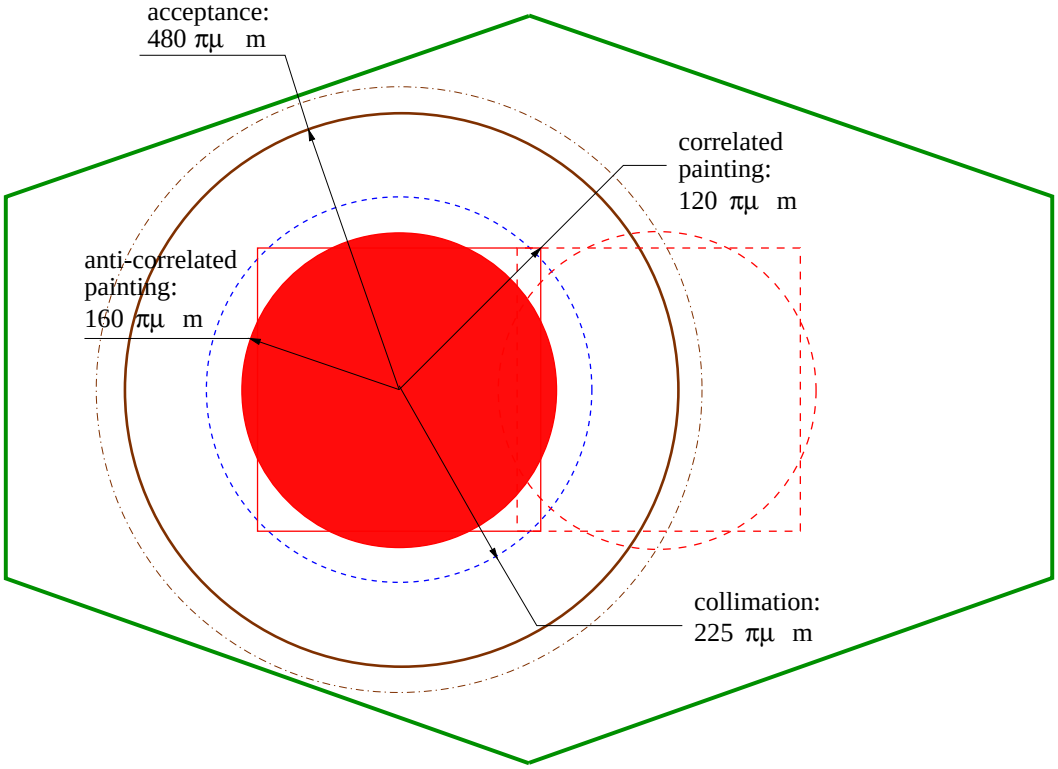

Figure 8: Schematic illustration of the beam emittance, collimation admittance, and vacuum chamber acceptance of the proposed hybrid lattice SNS ring. The green octagonal box indicates the vacuum chamber cross section (23 cm width, 15.2 cm height). The red squares correspond to off-momentum at $\Delta p/p$ of $\pm 1\%$. The ring magnet acceptance for the entire beam is 480 πmm·mr, the total transverse emittance is either 160 πmm·mr for anti-correlated and coupled painting or up to 240 πmm·mr for correlated painting. Ring collimation is planned at either 225 or 240 πmm·mr.

coupled (correlated) painting method, the final beam distribution on the mercury target is elliptical in the transverse plane. The total transverse emittance is 160 πmm·mr resulting in a space charge tune shift of about 0.15.

The two-stage collimation is performed at an acceptance from about 225 to 275 πmm·mr. The estimated beam tail at 225 πmm·mr is about 2×10^{-3}, and the collimation efficiency is about 95%. Thus, the total uncontrolled beam loss is about 10^{-4}. Alternatively, with correlated painting method the final beam distribution on the mercury target is rectangular in the

transverse plane. The beam is painted with both the horizontal and vertical emittance of up to 120 πmm·mr (total 240 πmm·mr). The two-stage collimation is performed at an acceptance from about 240 πmm·mr. The beam is susceptible to transverse coupling induced by space charge force and quadrupole roll misalignment. The estimated beam tail at 240 πmm·mr is about 10^{-2}, and the collimation efficiency is about 80%. Thus, the total uncontrolled beam loss is expected to be about 10^{-3}.

As shown in Table 3, the full momentum momentum spread is $\pm$0.7%. The momentum acceptance provided by the RF system of 40 kV voltage (harmonic h=1) is $\pm$1% at betatron acceptance of 480 πmm·mr. The physical aperture of the machine allows a momentum acceptance of more than $\pm$2% for a beam of 160 πmm·mr unnormalized emittance. In order to reach this value, chromatic sextupoles need to be activated to correct off-momentum optical mismatch.

Figure 9 shows the envelope of 480 πmm·mr acceptance at momentum deviation of 1% (upper), and 160 πmm·mr acceptance at momentum deviation of 2% (bottom), respectively, for the circulating beam. The acceptance of the extraction channel is 400 πmm·mr, and the acceptance of the RTBT is 480 πmm·mr.

2.2.4 Lattice and working points

At the nominal working point, the arc and the straight section lattice β function is matched, ensuring lowest possible β function in the arc for given cell length. Cell lengths of the arc and the straight sections are determined by the requirements of minimum space for injection, extraction and collimation, a low maximum β function (β_{max}), a low β_{max} to β_{min} ratio, and arc-straight matching. In addition, the horizontal betatron phase advance is 360 degrees across each arc section so that the dispersion function is zero in all the straight sections. The FODO arc structure is flexible for both chromatic correction and resonance corrections, while the long straight sections are flexible for injection and collimation. There is one power supply for the arc dipoles, and five power supplies for the lattice quadrupoles. Chromatic sextupoles are planned to be powered by four families of power supplies for nonlinear chromatic adjustments.

The FODO-doublet hybrid structure is flexible in tune adjustment for about 1 unit in both the horizontal and vertical directions. The alternative working points are (6.30, 5.27), (5.82, 4.80) and (5.82, 5.80). Figures 10 and 11 show the lattice functions for one super-period of the ring for the four working point candidates. Table 4 compares the advantage and disadvantage of these working points. Potential structure resonances are corrected by magnetic corrector packages (skew quadrupole, normal and skew sextupole, and octupole).

2.2.5 Injection and painting options

With the long straight section provided by the doublets, beam injection is essentially decoupled from lattice tuning. As shown in Figure 12, the fixed injection chicane is located between two nearby doublet quadrupole pairs. Figure 13 shows the two of the three painting schemes proposed for beam injection. Extra (50% beam size) vertical clearance is reserved in the injection section to accommodate anti-correlated orbit bumps for painting. Figure 14 shows beam tail development at the end of correlated painting. Table 5 compares the expected

Table 2: Evolution of beam parameters from Linac to the ring.

Quantity	Unit	HEBT	Ring	RTBT
Beam profile		Gaussian	quasi-uniform	quasi-uniform
Beam shape		round	round – round/rectang.	round/ rectang.
Emittance, ϵ_{UN} (rms)	π mm·mr	0.28	0.28 – 48	48
Emittance, ϵ_{UN} (99%)	π mm·mr	2.5	2.5 – 160	160
Machine acceptance	π mm·mr		480	480
Energy spread, $\Delta E/E$ (rms)	10^{-3}	0.5 – 3	4.2	4.2
Energy spread, $\Delta E/E$ (99%)	10^{-3}	1.5 – 6	12	12
Average current	mA	2	2	2
Peak current	A	0.054	0.032 – 40	40
D.C. current	A	20 – 0.6	0.6 – 96	96
Transverse S.C., $\Delta\nu/\nu$	%	34 – 1	1 – 2.5	2.5
Longitudinal S.C., V_{sc}	kV/turn		up to $\pm$ 16	

Table 3: Momentum aperture and sextupole improvement.

Item	Value
Beam momentum spread (99%)	$\pm$ 0.007
RF acceptance at 40 kV (h=1)	$\pm$ 0.010
Ring acceptance at nominal emittance	$\pm$ 0.015
Ring acceptance with sextupole correction	$\pm$ 0.020

Table 4: Comparison of tune working points for the hybrid lattice.

(Q_x, Q_y)	Advantage	Disadvantage	Correction
(6.30, 5.80)	perfect matching split tune ISIS operation high tunes	near $2Q_x + 2Q_y = 24$ (space charge) near $2Q_x = 12$	octupole
(6.30, 5.27)	perfect matching split tune CERN operation	near $3Q_y = 16$ near $2Q_y - Q_x = 4$ (sextupole) near $2Q_x = 12$	skew sextupole sextupole
(5.82, 5.80)	coupled painting away from integer AGS / Booster operation	large β_{max}/β_{min} coupling (square beam) loss-heavy for CERN $2Q_x - 2Q_y = 0$	 skew quadrupole octupole
(5.82, 4.80)	split tune away from integer AGS / Booster operation	large β_{max}/β_{min} near $2Q_y - Q_x = 4$ loss-heavy for CERN	 facing away sextupole

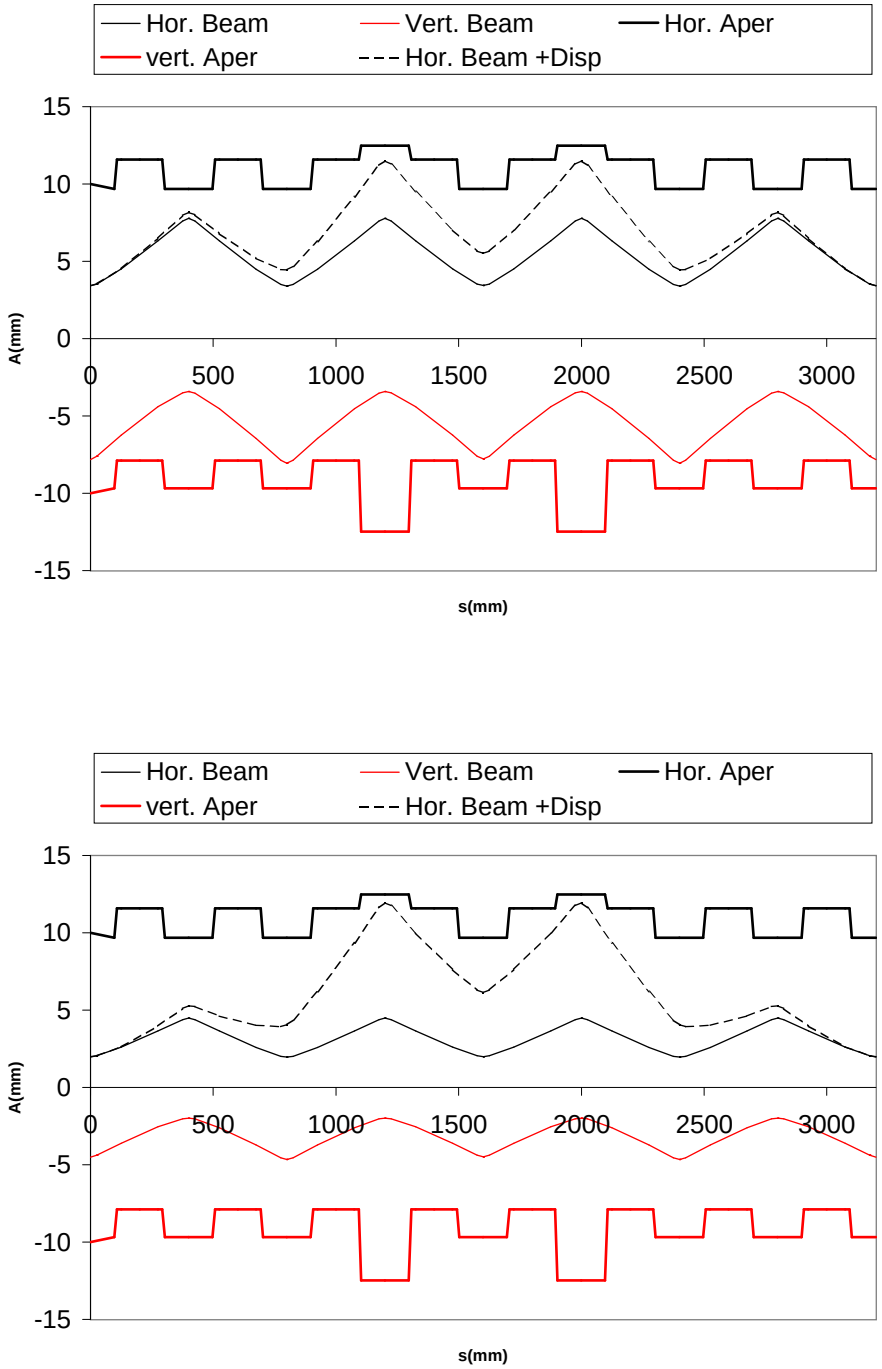

Figure 9: Envelope of 480 πmm·mr acceptance at momentum deviation of 1% (upper), and 160 πmm·mr acceptance at momentum deviation of 2% (bottom), in comparison with the vacuum chamber boundary. The solid lines indicate on-momentum value, and the dashed lines indicate off-momentum value.

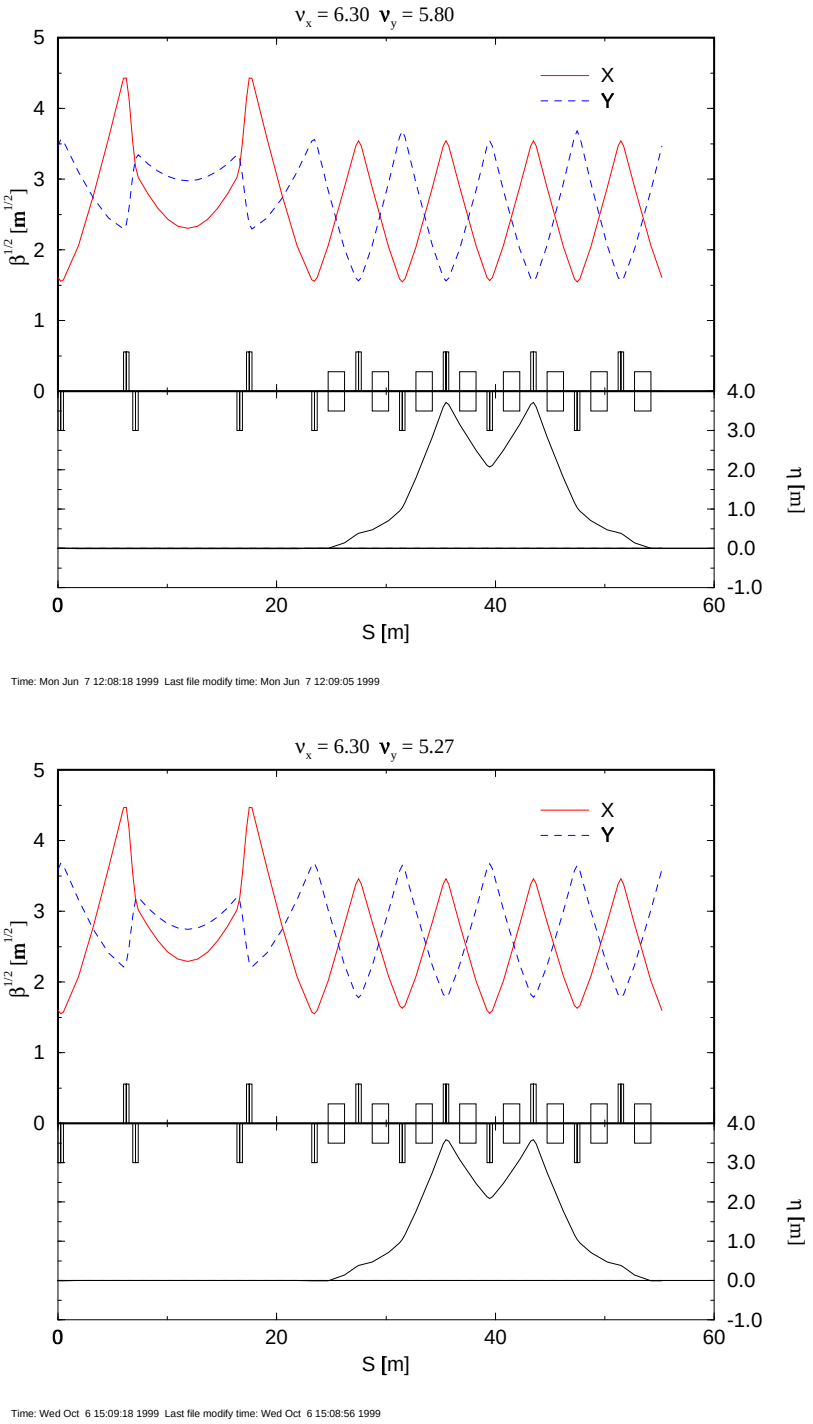

Figure 10: Lattice functions at tunes (Q_x, Q_y) of (6.30, 5.80) and (6.30, 5.27) for one superperiod of the proposed SNS ring.

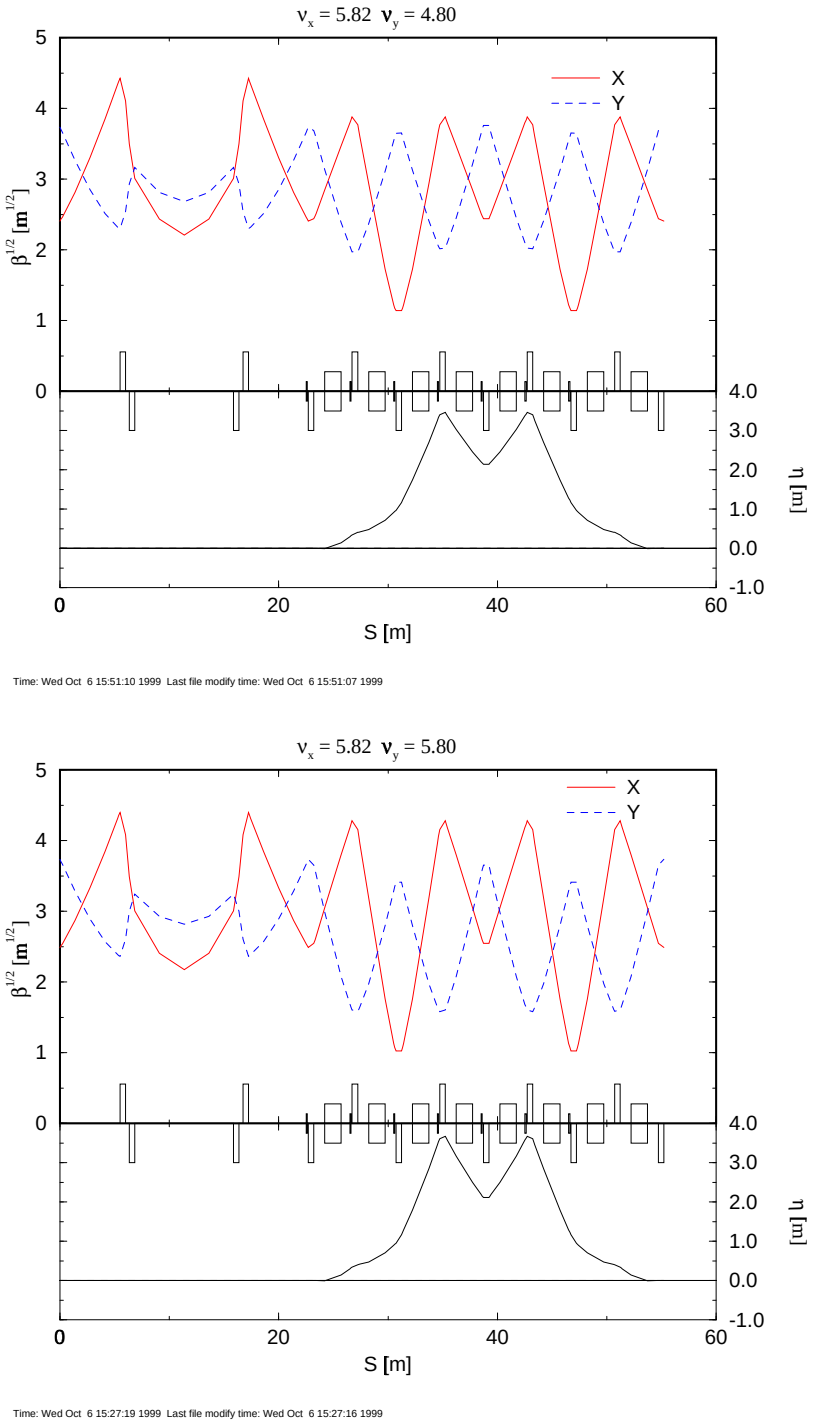

Figure 11: Lattice functions at tunes (Q_x, Q_y) of (5.82, 4.80) and (5.82, 5.80) for one superperiod of the proposed SNS ring.

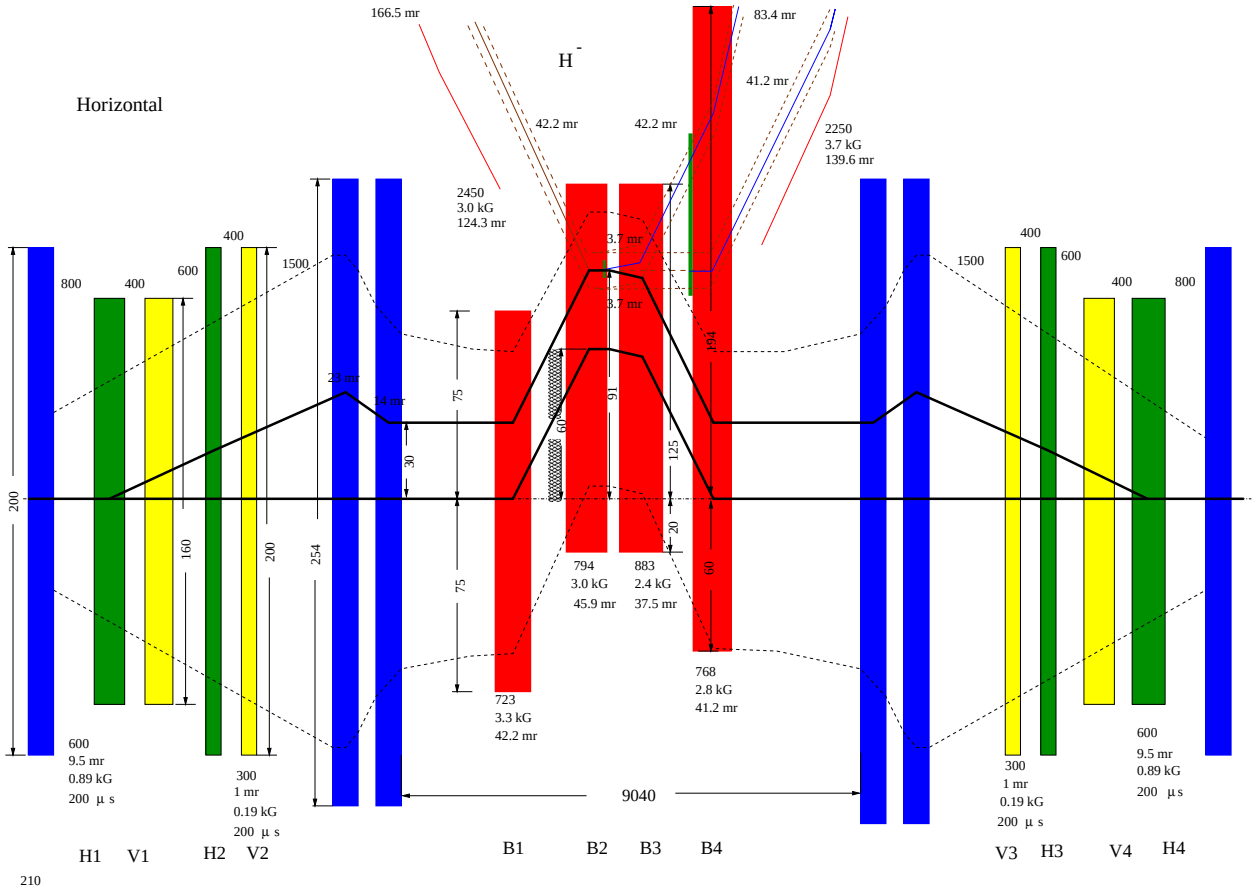

Figure 12: Schematic layout of the beam injection region of the proposed hybrid lattice ring.

performance of correlated, anti-correlated, and coupled-correlated painting schemes for beam injection. Programmable kickers are planned for the flexibility of dynamic orbit bumps for

Table 5: Comparison of injection schemes for the hybrid lattice.

Scheme	$\epsilon_x + \epsilon_y$ [πmm·mr]	Advantage	Disadvantage
Correlated	$120 + 120$	square shaped beam painting over halo	susceptible to coupling growth
Anti-correlated	160	round shaped beam K-V like distribution immune to coupling	extra 50% V aperture halo not painted over
Coupled H-V	$80 + 80$	painting over halo immune to coupling	requiring full coupling (unsplit tune / skew quad)

injection painting.

Figure 15 shows the transverse cross section at the location of injection stripping foil. Up to eight pieces of foil can be mounted on the adjustable foil rotation mechanism. The length of the foils can be adjusted to accommodate different painting schemes.

The stripper foil sits in a dipole magnetic field of 2.5 kG. As a consequence, stripped electrons will rotate about the magnetic field lines in a tight circle of radius $\rho = 1.23$ cm. To sweep these stripped electrons out of the ring without hitting (and further damaging) the foil, we take advantage of the fact that the foil sits in the downstream fringe field of its magnet: The electrons' center of gyration will travel downwards along a magnetic field line at a speed $\beta c \sin\alpha$, where α denotes the angle between the field line and the vertical at the point of injection. To ensure that the stripped electrons clear the lower edge of the foil on their first return, the injection C-magnet is designed so that $\alpha \geq 0.65$ mr. And to prevent the electrons being reflected back upwards by an effective mirror field, the lower pole face will not be chamfered. A grounded and water-cooled block of copper will catch the electrons.

Figure 16 shows the layout of the fixed injection chicane. The chicane is packed between two pairs of quadrupole doublets. The

2.2.6 Collimation and loss distribution

Immediately following the injection section is the multi-stage beam collimation section. This section consists of movable primary scatterers and three self-shielded collimators located in three consecutive drift spaces. Figure 17 shows expected collimation efficiency as a function of the available ring acceptance. At a design acceptance of 480 πmm·mr, the expected collimation efficiency is about 95%. Figure 18 shows the expected distribution of controlled and uncontrolled beam loss at various locations of the HEBT, ring, and RTBT assuming 2×10^{-3} beam halo [14, 15, 16, 17, 18] collected by the primary scatterer. Major uncontrolled beam loss is expected to be at the injection region caused by nuclear scattering of the foil, and from inefficiency of the collimation system. Beam residual in the gap between subsequent Linac

bunches is cleaned by the beam-in-gap (BIG) kicker together with the multi-stage collimation system.

2.2.7 Extraction

The accumulated beam in the SNS ring will form a single bunch ~590 ns long, with a gap of 250 ns. Extraction of the accumulated beam will happen soon after the injection process is completed (few hundred revolutions). and the beam will be extracted from the accumulator ring in a single beam revolution, and will last ~841 ns. The maximum extraction rate will be 60 Hz. The selected extraction scheme is to use a two-step process consisting of, first "kicking" the beam with fast kickers into a Lambertson type septum magnet and second, deflect the beam using the septum magnet into the extraction beam line (RTBT). The extraction system The extraction system will consist of 14 fast kickers (τ-200 ns) and a single Lambertson type septum magnet. The extraction will take place in one of the straight sections of the accumulator ring, with 7 kickers placed upstream of the quadrupole doublet and 7 kickers placed downstream of the doublet (Figure 19) followed by the septum magnet. Timing for extraction is very crucial. During the gap of the beam ($\tau \sim 250$ ns), the kickers will rise to their full strength required for extraction, and will remain on for ~600 ns until the beam is extracted from the accumulator ring into the Lambertson septum magnet. The kickers will deflect the beam vertically, and the Lambertson septum will deflect the beam horizontally in order to clear the quadrupole following the septum. The requirements for the extraction system are summarized in Table 6.

Table 6: Quadrupole magnet parameters for the proposed hybrid lattice SNS ring.

Parameter	Base Value	Comment
Extraction type	single-turn	two-step
Beam extraction gap	250 ns	
Maximum extraction rate	60 Hz	
First step:	14 kickers	full aperture
Kick strength	1.45 to 1.80 mr	vertical
Kicker rise-time	200 ns	0 to 97%
Second step:	Lambertson septum	
Lambertson deflection	16.8°	horizontal
Single kicker failure	beam on target	

The kickers will be made of ferrite core with rectangular cross-section (window frame). A single-turn copper conductor will be center-fed by one of the sides of the ferrite core. The length and the cross section of the ferrite of each kicker have been chosen in order to fulfill two requirements. First to reduce the maximum voltage and current which will power the kickers to level where the components can operate reliably, without the use of special insulation materials like oil. Second to allow the full beam to be extracted within the acceptance of the RTBT line and transported to target even with one of the kickers missing. The cross section of the fast kickers have been chosen in order to provide an acceptance of 480 πmm·mr during the

injection/accumulation period and an acceptance of 400 πmm·mr during the extraction. The same extraction acceptance of 400 πmm·mr applies also for the doublet quadrupoles between the kicker modules. The maximum vertical deflection of the central orbit of the beam at the entrance of the Lambertson will be 139 mm. This deflection corresponds to an acceptance of 400 πmm·mr at the entrance of the septum. The extraction parameters of the kicker modules are shown in Table 12.

The Lambertson Septum magnet The Lambertson septum magnet will be used to deflect horizontally by 16.8°, the fast beam from the accumulator ring. This beam deflection adequate for the beam to clear the quadrupole downstream of the septum. The parameters of the Lambertson septum magnet are shown in Table 13. The magnet which will run in a dc mode, will be designed to minimize the field (few Gauss) in the circulating beam region.

2.2.8 Magnets

Table 7 lists major parameters of the arc section dipole magnet. The peak field is chosen

Table 7: Dipole magnet parameters for the proposed hybrid lattice SNS ring.

Quantity	Value	unit
Dipole:		
bend angle	11.25	degree
number	32 + 1	used + reference
magnetic length	1.5	m
sagitta	3.85	cm
pole width	45	cm
gap height	17	cm
magnetic field	0.7406	T

to be moderate, as a compromise between the given space and cell length, the field quality of the magnet (fringe field and saturation), and the production cost. Table 8 lists the major parameters of the ring quadrupoles. The quadrupoles at the end of the 9-meter straight section drift space are designed to be of "figure of 8" to accommodate the clearance requirements of injection and extraction layout. The strength of the quadrupoles include a 10% margin that is adequate for the tuning of the lattice working point. Table 9 lists the major parameters of the chromatic sextupole magnets.

Major parameters for the injection magnets are listed in Table 10. The 3 kG field of the magnets INJSEPTM1 and INJBND2 is chosen to reduce pre-foil stripping of H^- ions to a level below 10^{-6} per meter, while the 2.4 kG field of the magnet INJBND3 is chosen to minimize the stripping of $n = 4$ and lower quantum state H^0 ions before the second stripping foil. The beam is injected with zero transverse momenta at the foil. The dynamic bump injection dipoles are places symmetrically in each 5.45-meter drift spaces. The power supply waveform of the dynamic bump magnets is designed to be programmable for the flexibility of manipulating the transverse beam profile to achieve the desired distribution required by the target. Table 11 lists main parameters of the dynamic bump kickers.

Table 8: Quadrupole magnet parameters for the proposed hybrid lattice SNS ring.

Quantity	Value	unit
Quadrupole:		
Regular ring quadrupole:		
number	28	
magnetic length	0.5	m
magnetic strength, $B'/B\rho$	0.82	m^{-2}
magnetic gradient	4.6	T/m
pole inscribed diameter	21	cm
peak field at pole tip	0.49	T
Large ring quadrupole:		
number	16	
magnetic length	0.6	m
magnetic strength, $B'/B\rho$	1.0	m^{-2}
magnetic gradient	5.6	T/m
pole inscribed diameter	26.4	cm
peak field at pole tip	0.73	T
Large narrow ring quadrupole:		
number	8	
magnetic length	0.5	m
magnetic strength, $B'/B\rho$	0.99	m^{-2}
magnetic gradient	5.6	T/m
pole inscribed diameter	26.4	cm
peak field at pole tip	0.74	T

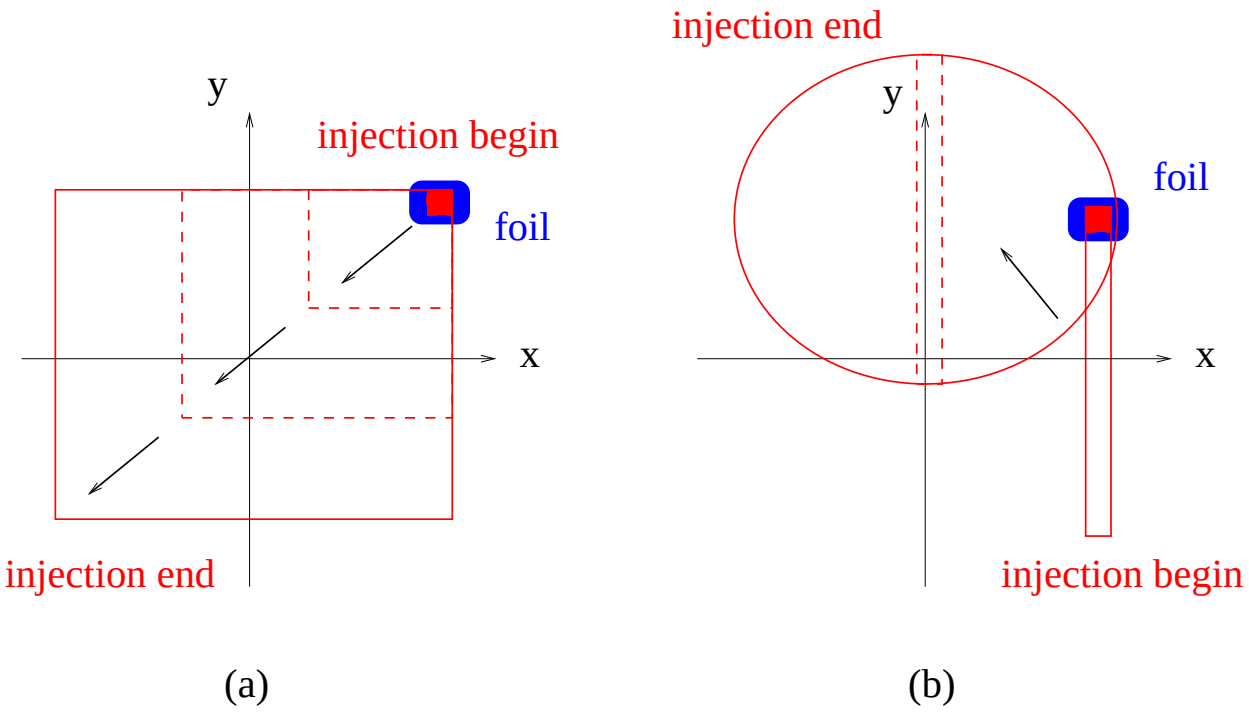

Figure 13: Correlated and anti-correlated painting injection schemes.

Table 9: Sextupole magnet parameters for the proposed hybrid lattice SNS ring.

Quantity	Value	unit
Sextupole:		
Regular ring sextupole:		
number	12	
magnetic length	0.2	m
magnetic strength, $B''/B\rho$	10	m^{-3}
magnetic gradient	57	T/m^2
pole inscribed diameter	21	cm
peak field at pole tip	0.31	T
Large ring sextupole:		
number	8	
magnetic length	0.2	m
magnetic strength, $B''/B\rho$	10	m^{-3}
magnetic gradient	57	T/m^2
pole inscribed diameter	26.4	cm
peak field at pole tip	0.49	T

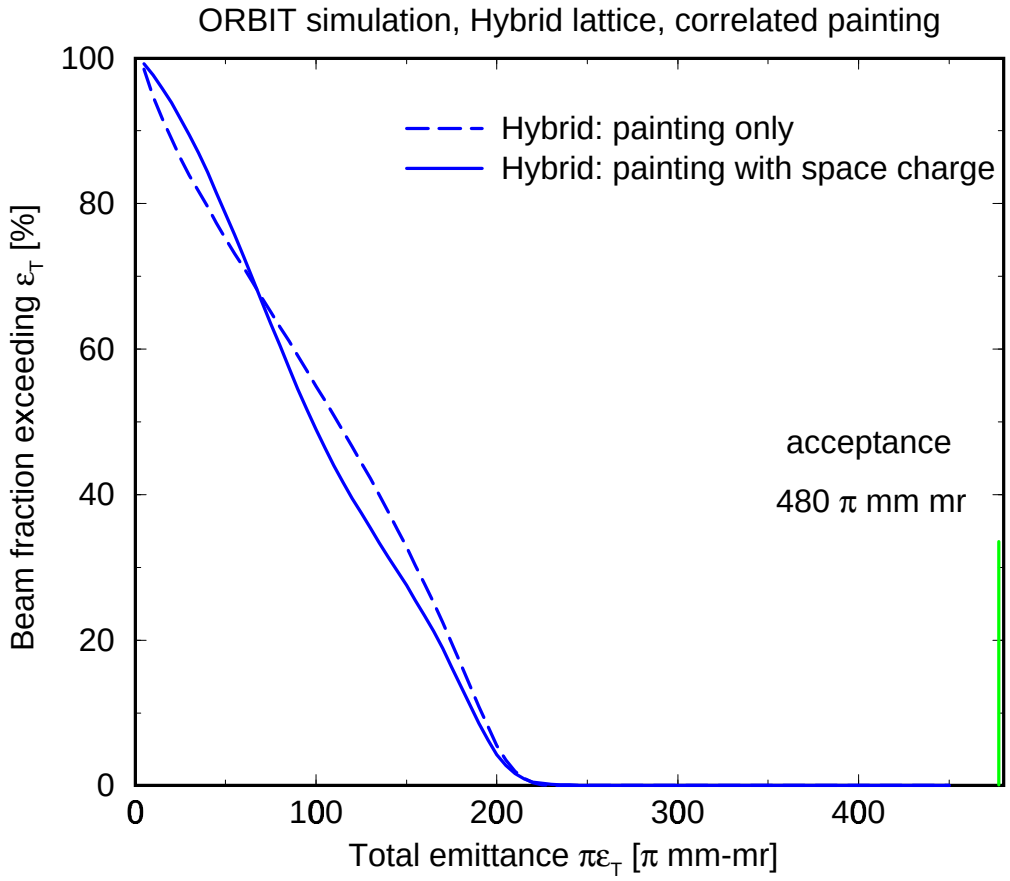

Figure 14: Fraction of the beam exceeding a given total transverse emittance at the end of injection painting. The simulation is performed with the ORBIT program incorporating space charge only. The beam exceeding the planned primary collimation at 240 πmm·mr is about 0.2%. Effects due to magnet field errors may cause more impact.

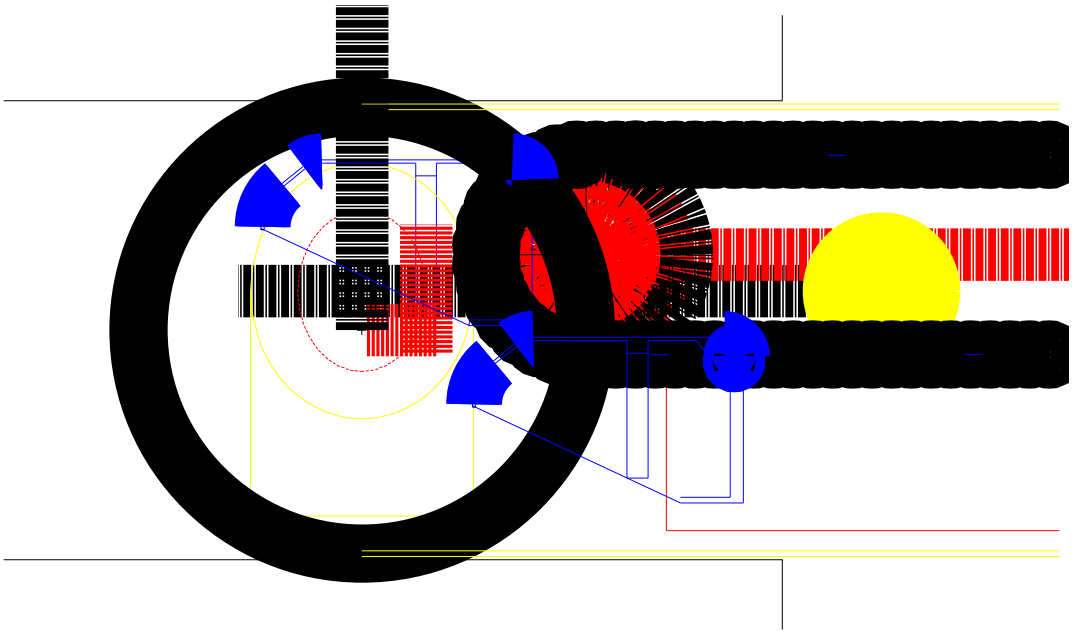

Figure 15: Injection foil mechanism for the proposed SNS ring.

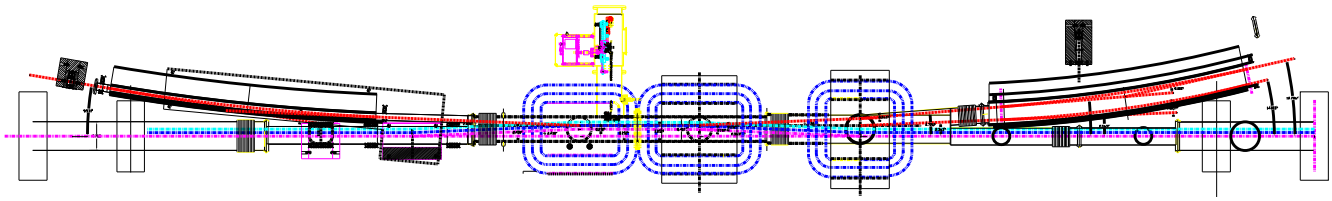

Figure 16: Layout of the fixed injection chicane.

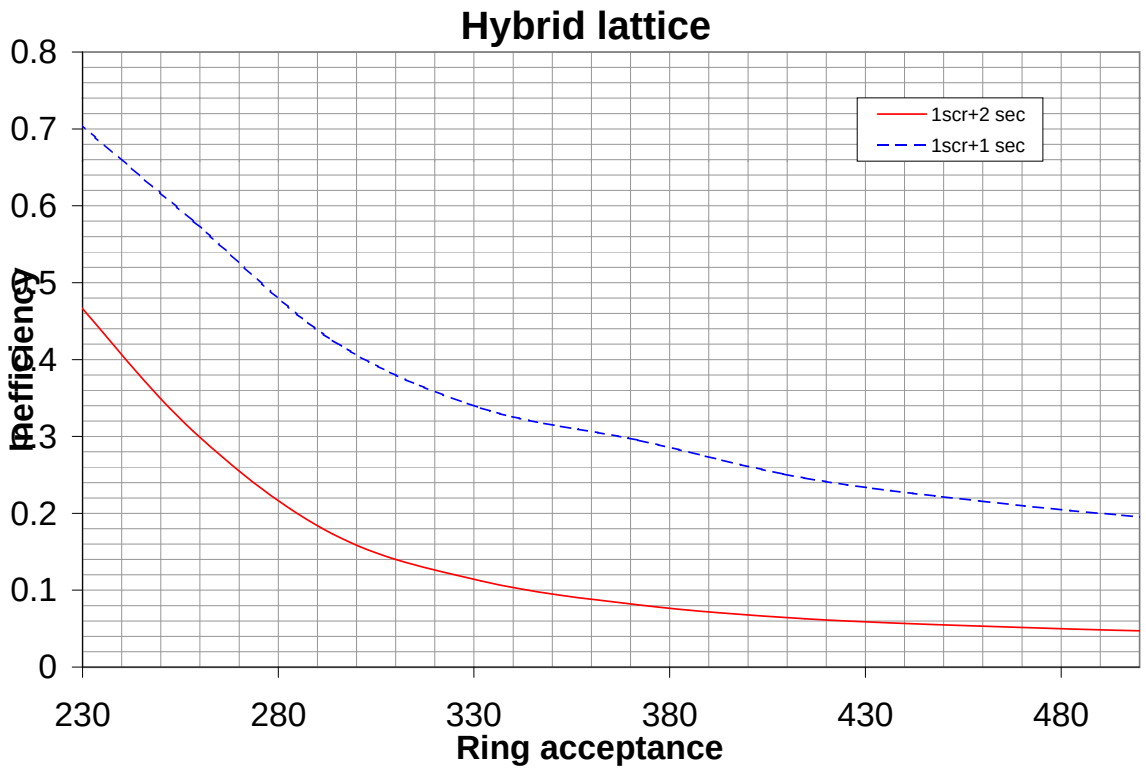

Figure 17: Comparison of collimation efficiency of the proposed SNS ring with one or two secondary collimators in addition to the primary scrapper. With two secondary collimators, the efficiency corresponding to the proposed acceptance of 480 πmm·mr is about 95%.

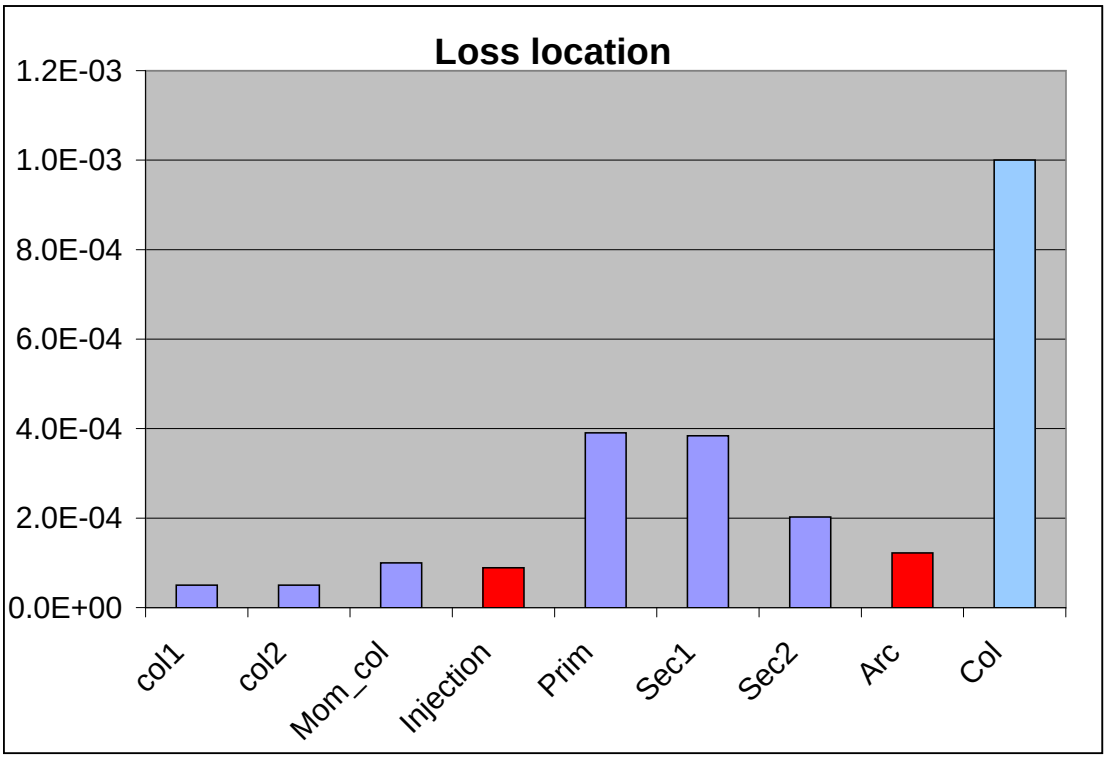

Figure 18: Expected controlled (purple), uncontrolled (red), and accidental (blue) beam loss at various locations of High-Energy-Beam-Transfer (HEBT) line, Ring, and Ring-to-Target-Beam-Transfer (RTBT) line.

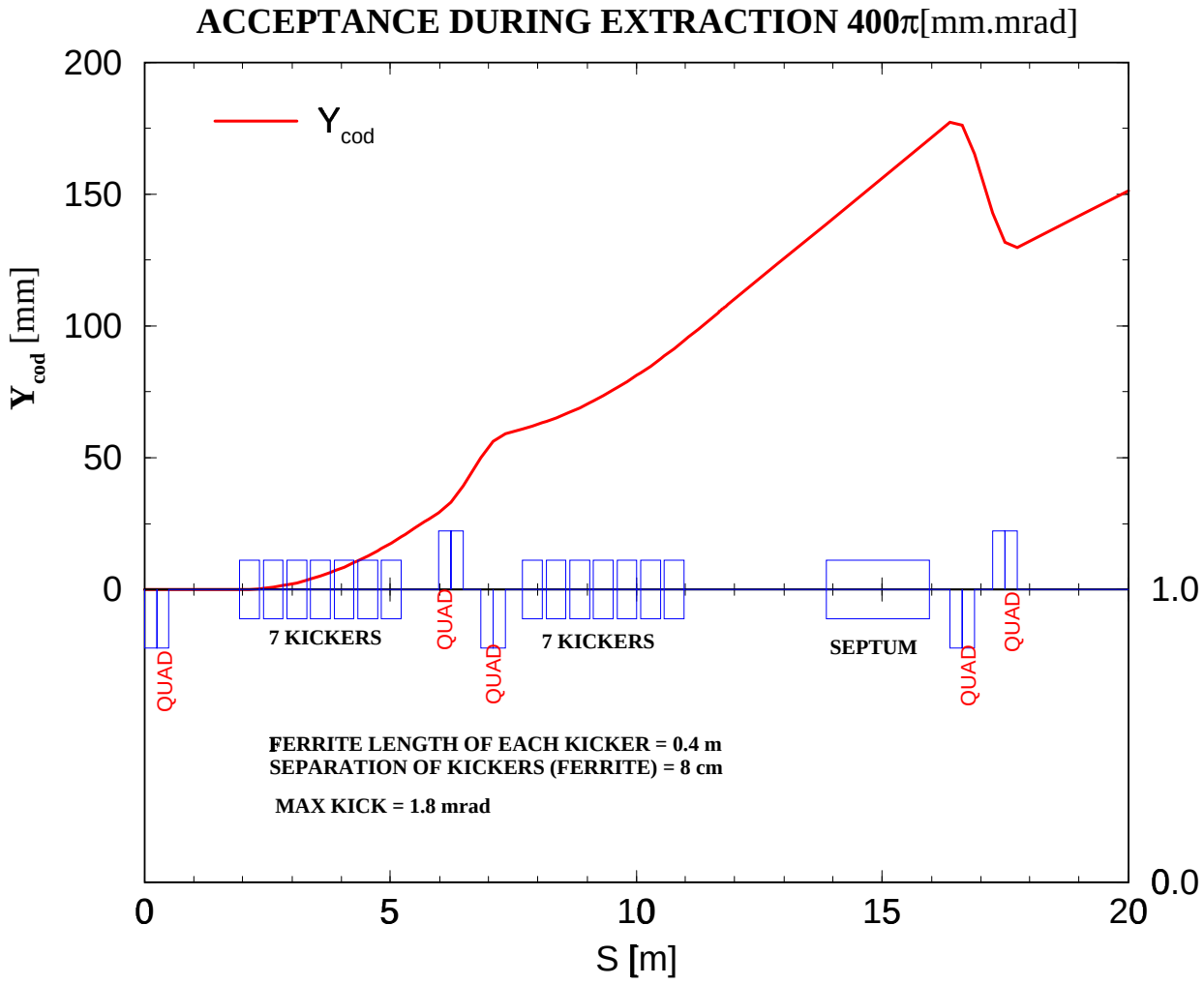

Figure 19: Hybrid lattice ring extraction layout and closed orbit.

Table 10: Injection DC magnet parameters for the proposed hybrid lattice SNS ring.

Quantity	INJSEPTM1	INJBND1	INJBND2	INJBND3	INJBND4	INJSEPTM2
Kick [mr]	124.3	42.2	45.9	37.5	41.2	139.6
Gap [cm]	5.1×6.1 (H×V)	20.6×15.1 (H×V)	22.2 (ID)	22.2 (ID)	25.4 (ID)	5×13.5 (H×V)
Core length [cm]	240.0	57.2	57.2	66.0	51.4	220.0
Effective length [cm]	245.0	72.3	79.4	88.3	76.8	225.0
No. of turns	2	10	36	36	36	2
B [kG]	3.0	3.3	3.0	2.4	2.8	3.7
I [kA]	6.3	5.5	1.5	1.2	1.7	7.8
Mag. res. [mΩ]	0.42	1.25	3.65	3.0	3.0	0.4
V_{dc} [V]	2.65	7.0	5.5	3.6	5.1	3.1
P_{max} [kW]	16.7	36.0	8.2	4.4	11.0	24.0

Table 11: Injection dynamic bump kicker parameters for the proposed hybrid lattice.

Parameter	Long module	Short module
Number	4	4
Kick [mr]	9.5, 6.7	1.0, 0.4
Field [kG]	0.79, 0.56	0.16, 0.06
Core length [m]	0.48	0.16
Effective length [m]	0.68	0.35
Gap (H×V) [cm]	20.6×23.5	20.6×23.5
Max. Current [A]	1298, 916	276, 110
Turns per coil	10	10
Coil resistance [mΩ]	3.39	2.67

Tables 12 and 13 summarize the specification of the extraction kickers and septum magnet. The acceptance of the extraction channel is 400 πmm·mr, and the acceptance of the downstream RTBT line is 480 πmm·mr. The expected beam loss at the extraction region is below 10^{-6}.

Table 12: Extraction kicker parameters for the proposed hybrid lattice SNS ring.

No. of kicker modules	14	
Length (ferrite)	0.4	m
Ferrite separation	0.08	m
Kicker strength	1.45 – 1.80	mr
Vertical displ. at septum entrance	139	mm
Maximum kicker voltage	34.5	kV
Maximum kicker current	3.0	kA

Table 13: Extraction Lambertson magnet parameters for the proposed hybrid lattice SNS ring.

Core length	2.1	m
Bending angle	16.8°	m
Field	8	kG
Gap (V)	14	cm
Width (H)	30	cm
Septum thickness	1	cm
No. of turns	60	
Maximum current	1500	A
Maximum V_{dc}	25	V
Coil resistance	0.0135	Ω

2.2.9 Expected magnetic errors and misalignments

Tables 14 and 15 list the expected integral magnetic errors of the ring dipole and quadrupole. The multipoles for the dipole magnet are extracted from the calculation of the design geometry. The multipoles for the quadrupole magnet are extracted and scaled from the measurement data of the AGS Booster magnets. Table 16 shows the expected misalignment based on the survey data of AGS Booster and the AGS-to-RHIC transfer line. Tables 17 and 18 show the contribution of dipole and quadrupole ends based on 3D field calculation.

2.2.10 Dynamic aperture

Dynamic aperture analysis for the hybrid lattice is not yet performed. However, based on the analysis of the original lattice, it is expected that with the compensated field harmonics and

Table 14: Expected magnetic errors of ring dipoles. The multipoles are normalized to 10^{-4} of the main field at the reference radius (R_{ref}) of 13 cm.

n	Normal		Skew	
	$\langle b_n \rangle$	$\sigma(b_n)$	$\langle a_n \rangle$	$\sigma(a_n)$
Body	[unit]			
2	-0.2	0.0	0.0	0.0
4	0.8	0.0	0.0	0.0
6	-0.8	0.0	0.0	0.0
8	-3.0	0.0	0.0	0.0
10	-4.4	0.0	0.0	0.0
12	-2.4	0.0	0.0	0.0

Table 15: Expected magnetic errors of ring quadrupoles. The multipoles are normalized to 10^{-4} of the main field at the reference radius R_{ref}. For regular ring quadrupoles, $R_{ref} = 10$ cm; for large ring quadrupoles, $R_{ref} = 12$ cm (approximately 92% of the quadrupole iron pole tip radius).

n	Normal		Skew	
	$\langle b_n \rangle$	$\sigma(b_n)$	$\langle a_n \rangle$	$\sigma(a_n)$
Body	[unit]			
2	0.0	-2.46	0.0	-2.5
3	0.0	-0.76	0.0	-2.0
4	0.0	-0.63	0.0	1.29
5	0.20	0.0	0.0	1.45
6	0.0	0.02	0.0	0.25
7	0.0	-0.63	0.0	0.31
8	0.0	0.17	0.0	-0.11
9	0.70	0.0	0.0	1.04
10	0.0	-0.06	0.0	-0.05
11	0.0	-0.22	0.0	-0.09
12	0.0	-0.06	0.0	0.08
13	-1.41	0.0	0.0	0.26
Ends	[unit·m]		(Length=0.15 m)	
6	0.25	0.0	0.0	0.0

Table 16: Expected alignment errors of ring magnets based on the survey measurement of the AGS Booster magnets and the AGS-to-RHIC transfer line magnets.

Item	Value
Integral field, magnet-to-magnet variation[a] (rms)	10^{-4}
Integral field, transverse variation[c] within R_{ref} (rms)	10^{-4}
Ring dipole sagitta deviation	3 cm
Magnetic center position[a,b] (rms)	0.1 – 0.5 mm
Magnet longitudinal position[b] (rms)	0.5 mm
Mean field roll angle[a,b] (rms)	0.2 – 1 mr

Table 17: Integrated dipole end field at one magnet end before pole tip end shimming, extracted from 3D TOSCA calculation. Normalized to 10^{-4} of the main field at the reference radius $R_{ref} = 13$ cm. The measurement radius is 7 cm.

n	Normal		Skew	
	$\langle b_n \rangle$	$\sigma(b_n)$	$\langle a_n \rangle$	$\sigma(a_n)$
1	0.1	–	0.0	–
2	51	–	0.0	–
3	0.5	–	0.0	–
4	−26	–	0.0	–
5	0.2	–	0.0	–

Table 18: Integrated quadrupole end field from one magnet end before pole tip end shimming, extracted from 3D TOSCA calculation. Normalized to 10^{-4} of the main field at the reference radius R_{ref}. For regular ring quadrupoles, $R_{ref} = 10$ cm; for large ring quadrupoles, $R_{ref} = 12$ cm (approximately 92% of the quadrupole iron pole tip radius).

n	Normal		Skew	
	$\langle b_n \rangle$	$\sigma(b_n)$	$\langle a_n \rangle$	$\sigma(a_n)$
2	0.4	–	0.0	–
3	0.1	–	0.0	–
4	0.7	–	0.0	–
5	121	–	0.0	–

corrected closed orbit, the dynamic aperture is near the physical aperture. Figure 20 shows the impact of misalignment and un-compensated error on the dynamic aperture obtained with computer program TEAPOT [19]. With the hybrid lattice, the sensitivity to the quadrupole misalignment is expected to be about a factor of 2 stronger due to the increased quadrupole strength.

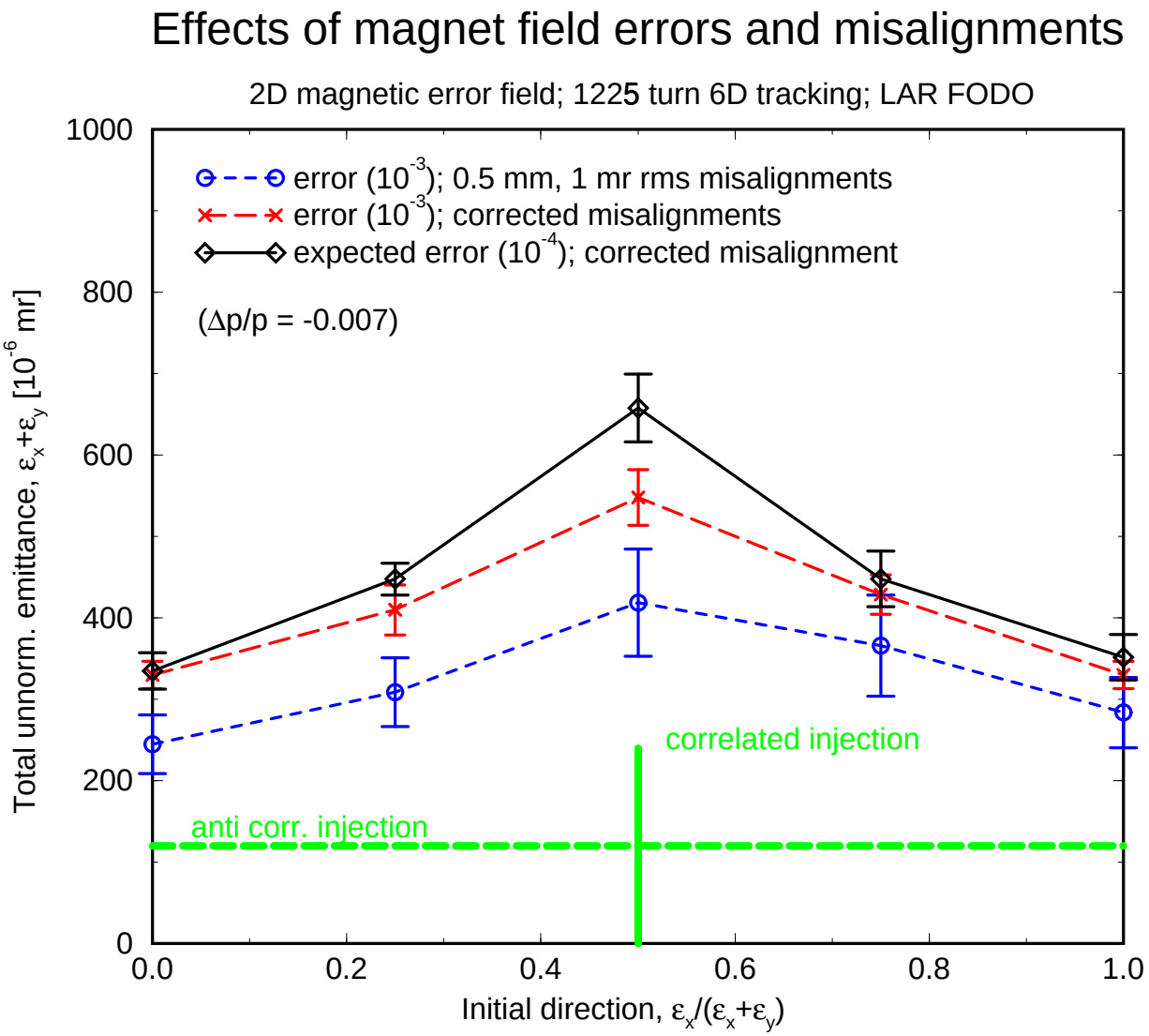

Figure 20: Dynamic aperture of the original FODO lattice obtained from 6-D TEAPOT computer tracking.

2.2.11 Impedance and instabilities

Impedance and instability analysis for the hybrid lattice is not yet performed. However, based on the scope of hardware change, changes on impedance budget and instability threshold are expected to be small [6, 20, 21].

2.3 Changes and Benefits

With essentially no change of the ring circumference and ring dipole magnet dimension, the acceptance of the machine is increased from 306 to 480 πmm·mr. Consequently, the collimation efficiency is increased from about 80% to 95%. The expected uncontrolled beam loss is reduced from 10^{-3} to 10^{-4} level. In addition, the long uninterrupted straight section provides flexibility for injection, collimation, and other arrangements. Table 18 summarizes the major change of parameter of the ring, HEBT, and RTBT lines.

Table 19: Major change for the SNS ring between the original all-FODO lattice (July 1999) and the proposed hybrid lattice design.

Quantity	All-FODO	Hybrid	unit
Circumference	220.688	220.88	m
Acceptance	306	480	πmm·mr
Extract. acceptance	360	400	πmm·mr
Maximum β in arc	19.2	12.6	m
Maximum D_x in arc	4.1	3.7	m
Injection scenario	correlated	anti-corr. or coupled / corr.	
Beam shape $(x-y)$	rectangular	elliptical / rectang.	
Total emittance	120+120	160 / 120+120	πmm·mr
Collimator acceptance	240	225 / 240	πmm·mr
Collimation Efficiency	$\sim$ 80	95 / $\sim$ 90	%
Space charge tune spread $\Delta\nu_{sc}$	0.20	0.15 / 0.20	
Beam tail fraction	$\sim 10^{-2}$	$\sim 2\times10^{-3}$ / 10^{-2}	
Expected beam loss	$\sim 2\times10^{-3}$	$\sim 10^{-4}$ / 10^{-3}	
Straight section space	4 × 5.2	9.04, 2 × 5.45	m
Quad. ID	21, 31	21, 26	cm
Number of quads. (ring)	48	52	
Injection DC dipole	3	4	
Extraction kicker module	8	14	
Number of quads. (HEBT)	34	35	
Number of quads. (RTBT)	28	32	
(Extra quad, Ω layout, RTBT)	–	4	
Quad power supply (HEBT)	21	24	
Quad power supply (RTBT)	16	23	
(Extra quad PS, Ω layout, RTBT)	–	4	

2.3.1 Ring lattice and layout

The ring circumference and footprint remains essentially the same. However, the four straight sections are changed from FODO to doublet structure. A better matching between the arc and the straight section reduces the maximum β function in the arc from 19.2 m to 12.6 m,

and dispersion from 4.1 m to 3.7 m. The ratio between maximum and minimum β is reduced from about 14 to 7.5 across the entire ring.

The length of the uninterrupted straight section is increased from about 5.2 to 9.0 meters. Instead of four drift sections of 5.2 m each, each straight section consists of one 9.04 m and two 5.45 m drift sections.

The location of the arc dipoles are changed to the center of each half cell, instead of 0.55 m from the center, thus further reducing the β function at the arc dipoles. Each arc quadrupole is accompanied by a sextupole on one side and a corrector on the other side, both of them near optimum location of maximum β.

The nominal working point in the tune space is changed from (5.82, 5.8) to (6.30, 5.80). The horizontal and vertical tunes are split by half a unit to reduce the impact of transverse coupling caused by space charge and magnet misalignments. The proposed lattice is similarly flexible in tune adjustment. The alternative working points are (6.30, 5.27), (5.82, 4.80) and (5.82, 5.80).

2.3.2 Ring acceptance

Due to reduction of the maximum β function in the arc, the acceptance of the arc is increased from about 306 πmm·mr to 570 πmm·mr at $\pm 0.7\%$ momentum deviation. The ring acceptance is limited by the minimum acceptance at the injection and extraction straight sections, which is increased from less than 360 to 480 πmm·mr. The gain in acceptance is achieved with minimum change of the magnet dimensions.

The acceptance of the extraction channel is increased from about 360 to 400 πmm·mr. The acceptance of the RTBT remains 480 πmm·mr.

2.3.3 Injection scheme

Flexibility in injection design is essential in reducing uncontrolled beam loss. With the original design, the fixed injection chicane spreads across 2 drift spaces of 5.2 m each. Both the injection H^- and stripped H^0 beam have to pass the lattice quadrupole, making machine operation less robust. With the proposed design, the fixed injection bump is confined in a 9 m long drift section between two nearby lattice quadrupoles. The injection foil is located near the middle of the doublet drift section where derivative of the β function is near zero.

With the original design, only correlated injection bump can be accommodated, allowing the Linac beam to be painted to a rectangular shape in the transverse physical space. Such a beam is susceptible to emittance growth caused by the transverse coupling, especially when the horizontal and vertical tunes are near at the design working point of (5.82, 5.80). With the proposed design, both correlated and anti-correlated injection bumps can be accommodated. With the anti-correlated scheme, the Linac beam is painted to a K-V like distribution which is elliptical in the transverse physical space. The beam is almost immune to the transverse coupling, especially when the tunes are split at (6.30, 5.80).

2.3.4 Space charge tune shift and beam tail

With the original design, the beam is painted to a transverse emittance of 120 πmm·mr in both the horizontal and vertical directions (total maximum 240 πmm·mr). Correspondingly, the space charge tune spread is about 0.2. The estimated fraction of beam tail is about 2% at the acceptance of primary collimation (240 πmm·mr). With the proposed design, the beam is painted with the anti-correlated scheme to a transverse emittance of total 160 πmm·mr. The corresponding space charge tune spread is about 0.15. The estimated beam tail is significantly reduced at the admittance of primary collimation (225 πmm·mr).

2.3.5 Collimation efficiency and uncontrolled beam loss

With the original design, the difference between the vacuum chamber acceptance (306 πmm·mr) and collimation acceptance (240 πmm·mr) is small. The collimation efficiency is limited to about 80%. With the proposed design, the acceptance difference (480 πmm·mr ring acceptance vs. 225 πmm·mr collimator acceptance) is significantly increased. Also, the long straight sections of the new lattice provide much more freedom for the choice of collimator location. Secondary collimators can be located at optimum phase advance from the primary. Consequently, the collimation efficiency is increased from 80% to about 95%.

2.3.6 Ring magnets and power supplies

For the ring lattice dipole, the physical dimension (vertical 17 cm gap), strength, and power supply specification all remains the same.

The large aperture (31 cm ID) quadrupoles in both the arc and the straight section have been eliminated. Instead, aperture of the quadrupoles at both the maximum dispersion region and the doublet region is chosen to be 26 cm. Aperture of the regular quadrupoles (21 cm ID) remains the same. The number of power supplies for the ring lattice quadrupole (5) remains the same, but the strength for the 26 cm ID quadrupoles is increased to meet the doublet specification.

2.3.7 Injection and extraction magnets

With the original design, the fixed injection chicane consists of three dipoles and one quadrupole. With the proposed design, the chicane consists of four dipoles of increased transverse dimension to accommodate anti-correlated painting with increased acceptance (from about 360 to 480 πmm·mr). The number of dynamic bump dipoles for injection painting remains the same (8), but their length and transverse dimension are changed.

The number of extraction kicker modules is increased from 8 to 14. The increase is partly due to the change of the straight section quadrupole layout, and partly due to the increased acceptance of the circulating beam in the extraction section (from about 360 to 480 πmm·mr). The acceptance of the extraction channel is increased from 360 to 400 πmm·mr.

2.3.8 Vacuum chamber

The vacuum chamber design is different in the proposed design, but the level of effort remains similar.

2.3.9 HEBT

The last cell of the HEBT line is changed from FODO to doublet structure to match the ring straight section lattice. One additional quadrupole and two additional quadrupole power supplies are needed to fulfill the matching. Note that the third power supply is needed due to the change of collimation scheme.

2.3.10 RTBT

The change in RTBT magnets and power supplies is mainly due to the need to accommodate the configuration change from the alpha to the omega layout. The number of lattice cells before the bend in RTBT is increased from 4 to 6 cells to provide achromat dispersion cancelation. Instead of having the same cell length, the RTBT for the omega configuration consists of two types of cells (7.7 m and 11.5 m cell length). Four extra quadrupoles and five extra power supplies are needed to fulfill the function.

An alternative RTBT scheme for the omega configuration is to keep the same cell length (11.5 m) and number of cells, increasing the number of cells (from 4 to 6) in the achromat while reducing the number of cells in the later transport section. The extra four quadrupoles are no longer needed, and the extra power supplies can be reduced. However, 26 cm ID quadrupoles instead of 21 cm ID quadrupoles need to be used in the achromat, and the target footprint will be slightly changed.

The change in RTBT due to hybrid lattice alone is similar to that of the HEBT line.

3 Itemization of Changes

3.1 Ring quadrupole and power supply

Table 20: Comparison between the original all-FODO lattice and the proposed hybrid lattice on quadrupole and power supply requirements for the ring. The change is indicated by the parenthesis indicating proposed (original) value.

Magnet	Type	Location	Number of magnets	Number of power supplies
Quad.	21Q40	arc, straight	28 (40)	2, share 1 (4)
	31Q50	arc, straight	0 (8)	0 (1, share 1)
	26Q60	arc, straight	16 (0)	2 (0)
	26QN50	straight	8 (0)	1 (0)

3.2 Ring injection chicane

Table 21: Injection DC magnet parameters for the original SNS ring.

Quantity	INJSEPTM1	INJBND1	INJBND2	INJBND3	INJSEPTM2
Kick [mr]	132.5	27.9	41.4	13.5	177.0
Gap [cm]	3×8	17×20	20×30	17×20	5×10
Effective length [cm]	250	50	78.1	50	200
No. of turns	4	24	24	16	4
B [kG]	3.0	3.2	3.0	1.5	5.0

Table 22: Injection DC magnet parameters for the proposed hybrid lattice SNS ring.

Quantity	INJSEPTM1	INJBND1	INJBND2	INJBND3	INJBND4	INJSEPTM2
Kick [mr]	124.3	42.2	45.9	37.5	41.2	139.6
Gap [cm]	5.1×6.1 (H×V)	20.6×15.1 (H×V)	22.2 (ID)	22.2 (ID)	25.4 (ID)	5×13.5 (H×V)
Effective length [cm]	245.0	72.3	79.4	88.3	76.8	225.0
No. of turns	2	10	36	36	36	2
B [kG]	3.0	3.3	3.0	2.4	2.8	3.7

3.3 Ring injection dynamic bump

Table 23: Comparison between the original all-FODO lattice and the proposed hybrid lattice on dynamic bump magnets.

Quantity	Original	Proposed	Units
No. of kicker s	8	8	
Core length	0.34	0.16, 0.48	
Effective length	0.5	0.35, 0.68	m
Kicker strength	0.5 – 8	0.1 – 9.5	mr
Field	0.06 – 0.9	0.1 – 0.9	kG
Gap	17×17	20.6×23.5	cm
Max. Current	100 – 1230	110 – 1298	[A]
Number of turns	10	10	

3.4 Ring extraction kicker and Lambertson

Table 24: Comparison between the original all-FODO lattice and the proposed hybrid lattice on extraction kicker magnet.

Quantity	Original	Proposed	Units
No. of kicker modules	8	14	
Total length	1.9, 1.9	3.28, 3.28	m
Kicker strength	2.1	1.45 – 1.80	mr
Gap (H)	11.5	10.0 – 17.5	cm
Width (V)	12.9 – 15.4	11.7 – 22.0	cm

Table 25: Comparison between the original all-FODO lattice and the proposed hybrid lattice on extraction Lambertson magnet.

Quantity	Original	Proposed	Units
Core length	3.1	2.1	m
Bending angle	15.5°	16.8°	m
Field	5	8	kG
Gap (V)	14	14	cm
Width (H)	16	30	cm
No. of turns	40	60	
Maximum current	1400	1500	A
Maximum V_{dc}	15	25	V
Coil resistance	0.009	0.0135	Ω

3.5 Ring vacuum chamber

The new layout reduces the number of quadrupole chambers, flanges and bellows in the straight sections, but increase the types of arc half-cell chambers from two to four. The reduction of the large quadrupole aperture from 30 cm to 26 cm eases the chamber transition. Overall, the cost and level of design effort remain similar.

The arc vacuum chambers, covering from QVX1 to QVX9 as shown in Figure 7, will consist of eight half-cell chambers and one quadrupole chamber. The half-cell chamber is approximately 4 meters long, containing chambers for dipole, bellows, quadrupole and BPM. The available beam-stay-clear aperture in the whole arc is approximately 20 cm except at Q4 and Q6 where the aperture is close to 25 cm.

The chambers will be jointed to each other with 10" Conflat flanges except between D3 and Q4 where 12" Conflat will be utilized. Two 8" Conflat ports will be provided at mid-plane of each half-cell chamber for pumps. Smaller ports will be provided for vacuum instrumentation.

One chamber with BPM will be used for the each doublet at straight sections. Evac type quick disconnect flanges will be used to join to chambers of accelerator components such as RF, collimators and injection and extraction equipment.

3.6 HEBT

Table 26: Comparison between the original all-FODO lattice and the proposed hybrid lattice on magnet and power supply requirements for HEBT. The change is indicated by the parenthesis indicating proposed (original) value.

Magnet	Type	Location	Number of magnets	Number of power supplies
Dipole	8D500	Achromat	5	1
	8D500	Achromat	1	1
	8D250	ARMS	1	1
	12C20	LAMS, ARMS, L-dump	12	12
	20C30	Achromat	4	4
Quad.	12Q50	LAMS, ARMS	22 (21)	16 (13)
	21Q40	LAMS	1	1
	21Q40	Achromat	6	3
	12Q50	L-dump	6	4

3.7 RTBT

Table 27: Comparison between the original all-FODO lattice and the proposed hybrid lattice in omega configuration on magnet and power supply requirements for RTBT. The change is indicated by the parenthesis indicating proposed (original) value.

Magnet	Type	Number of magnets	Number of power supplies
Dipole	17D310	1	1
	20C30	14	14
	36C30	2	2
	17DV50	1	1
Quad.	21Q40	25 (23)	16 (11)
	36Q80	5	5
	26Q50	2 (0)	2 (0)

4 Impact on the Front End and Linac

There is no noticeable impact on both the front end and the Linac. Table 9 shows major Linac/HEBT interface parameters.

Table 28: Linac requirements and Linac/HEBT interface parameters.

Quantity	Value	unit
Energy, E_k	1000	MeV
Average current	2.2	mA
Repetition rate	60	Hz
Peak current	$\sim$56	mA
Emittance (normalized, rms)	0.45	π mm mr
Transverse halo (5σ)	10^{-4}	
Beam energy jitter (99.99%)	$\pm$ 2.2	MeV
Energy spread (rms)	0.33	MeV
Beam gap residual	10^{-4}	

5 Impact on the Target

The ring and RTBT is expected to deliver elliptically shaped beam to the target, although rectangular beam is also possible. The aspect ratio is adjustable to accommodate the desired target size. Both correlated and anti-correlated painting are expected to satisfy the required current density limit of below 0.25 A/m^2.

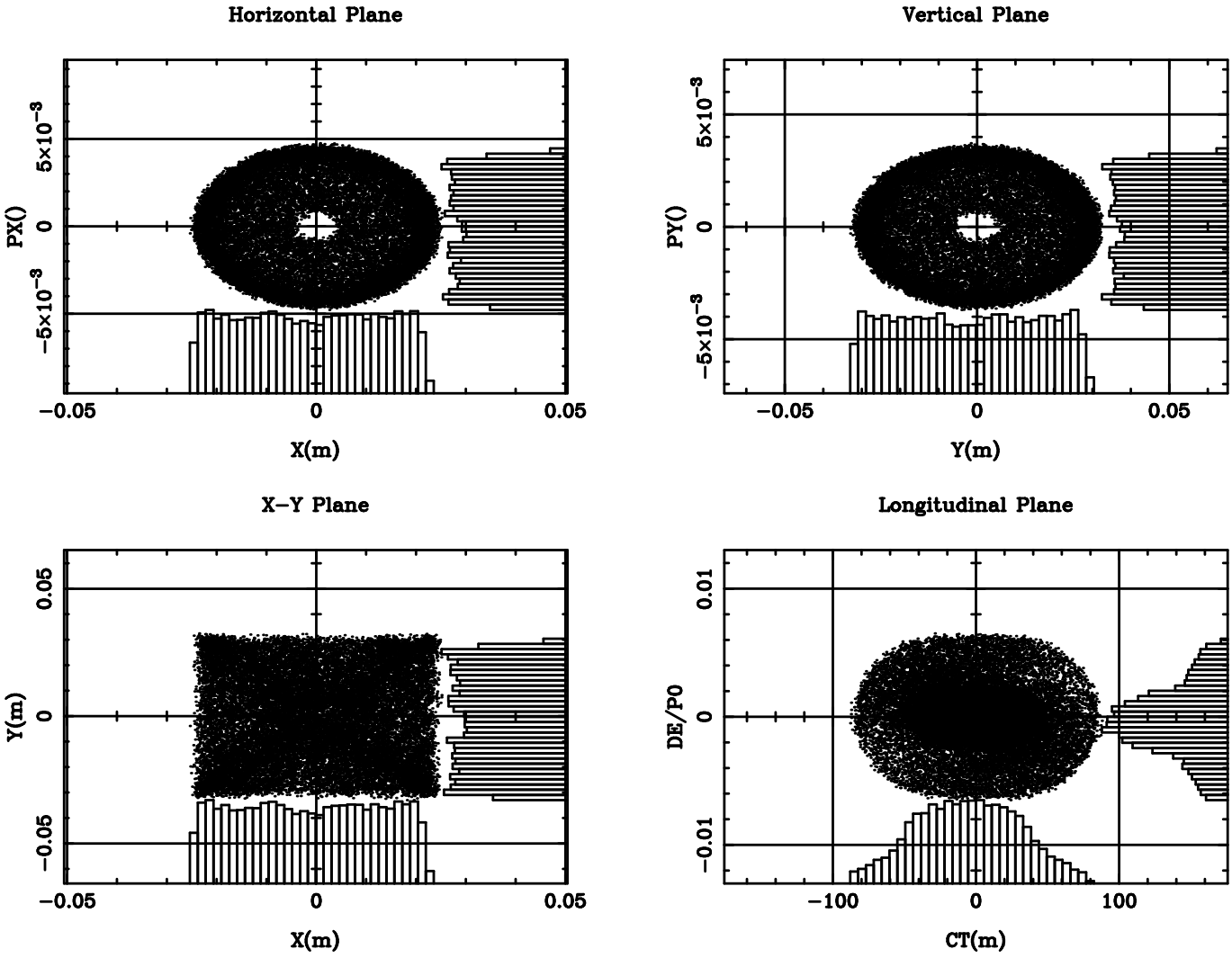

Figure 21: Beam distribution with correlated painting.

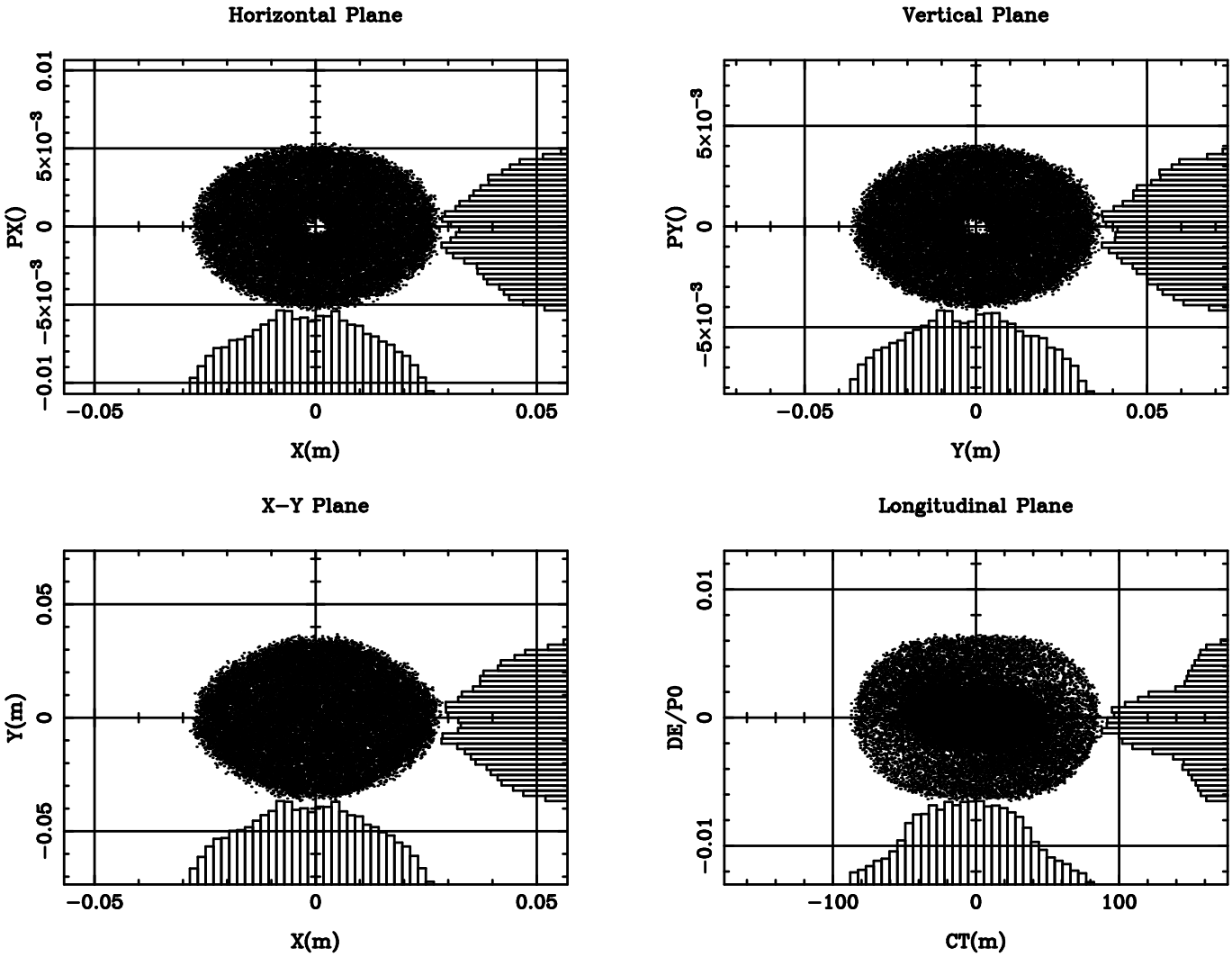

Figure 22: Beam distribution with anti-correlated painting.

6 Impact on the Ring WBS

The total increase in cost in mechanical and electrical systems is $ 2,447,470, excluding overhead and contingency. The cost increase for mechanical systems is $ 869,219, and for electrical systems is $ 1,578,251.

6.1 Mechanical Systems

Table 29: HEBT magnets (WBS 1.5.1.1.2).

July 99 Review	Present	Cost
HEBT Quadrupoles	HEBT Quadrupoles	Increase ($)
27 each 12Q50 magnets	28 each 12Q50 magnets	
$ 1,084,993	$ 1,113,688	$ 28,695

Table 30: HEBT magnets (WBS 1.5.1.1.3).

July 99 Review	Present	Cost
HEBT Correctors	HEBT Correctors	Increase ($)
12 each 14C20 magnets	13 each 14C20 magnets	
$ 282,863	$289,943	$ 7,080

Table 31: Injection septum (WBS 1.5.2.3.1).

July 99 Review	Present	Cost
Injection magnet	Injection magnet	Increase ($)
1 each septum magnet	1 each septum magnet Re-design effort	
$378,204	$387,029	$8,825

This increase is for the omega configuration with the hybrid lattice. All changes, except for the increase for a change in number for RTBT 21Q40 quadrupoles ($117,418 cost increase), are required solely for the hybrid lattice.

Hybrid Lattice increase: $ 751,801

Omega increase: $ 117,418

Total Increase in Mechanical Systems = $869,219

Table 32: Injection stripper dipole (WBS 1.5.2.3.5).

July 99 Review	Present	Cost
Chicane/foil Dipole magnets	Chicane/foil Dipole magnets	Increase ($)
1 each 20D50 magnet	2 each 20D50 magnet	
	Re-design effort	
$248,751	$311,156	$62,406

Table 33: Injection foil change drive (WBS 1.5.2.5.1).

July 99 Review	Present	Cost
Injection Foil Drive	Injection Foil Drive	Increase (K$)
1 Unit	1 unit	
	Re-design effort	
$344,730	$356,718	$ 11,988

Table 34: Ring Magnets (WBS 1.5.3.1.1).

July 99 Review	Present	Cost
HEBT, Ring, RTBT Quadrupoles	HEBT, Ring, RTBT Quadrupoles	Increase (K$)
32 Units 17D140	32 Units 17D140	
	Re-design effort	
$3,954,143	$3,984,458	$ 30,315

Table 35: Ring Magnets (WBS 1.5.3.1.2).

July 99 Review	Present	Cost
HEBT, Ring, RTBT Quadrupoles	HEBT, Ring, RTBT Quadrupoles	Increase (K$)
69 Units 21Q40	60 Units 21Q40	
$2,646,750	$2,410,728	($ −236,022)

Table 36: Ring Magnets (WBS 1.5.3.1.3).

July 99 Review	Present	Cost
Ring Quadrupoles	Ring, RTBT Quadrupoles	Increase (K$)
9 Units 31Q42	9 Units 26QN50	
	18 Units 26Q60	
	Re-design	
$723,474	$1,449,184	$ 725,710

Table 37: Ring Magnets (WBS 1.5.3.1.4).

July 99 Review	Present	Cost
Ring Sextupoles	Ring Sextupoles	Increase (K$)
24 Units 24S20	12 Units 21S20 8 Units 26S20	
$936,778	$874,002	($ −62,776)

Table 38: Ring Magnets (WBS 1.5.3.2.1).

July 99 Review	Present	Cost
Ring Quadrupoles	Ring, RTBT Quadrupoles	Increase (K$)
56 26CM30 15 26C30	43 26CM30 28 26C30 Re-design	
$1,185,750	$1,194,059	$ 8,309

Table 39: Ring Magnets (WBS 1.5.3.2.2).

July 99 Review	Present	Cost
Ring Quadrupoles	Ring, RTBT Quadrupoles	Increase (K$)
8 36CM30 6 36C30	15 31CM30 6 36C30 Re-design	
$580,322	$718,579	$138,257

Table 40: Extraction Pulsed Magnets (WBS 1.5.9.1).

July 99 Review	Present	Cost
Ring Quadrupoles	Ring, RTBT Quadrupoles	Increase (K$)
8 14DP40	14 14DP40 Re-design	
$630,914	$777,346	$146,432

6.2 Electrical Systems

Table 41: HEBT Power Supplies (WBS 1.5.1.2.1).

July 99 Review	Present	Cost
Power Supplies	Power Supplies	Increase ($)
3 Dipoles, 17 Quads, Linac Dump-4 Quads Power: 494 kW	3 Dipoles, 20 Quads, Linac Dump-4 Quads Power: 567 kW	
$ 1,625,225	$ 1,711,225	$ 86,000
Cables: $ 164,100	$ 183,035	$ 18,935

Table 42: Injection DC Power Supplies (WBS 1.5.2.4).

July 99 Review	Present	Cost
Power Supplies	Power Supplies	Increase ($)
5 Power Supplies Power: 260 kW	6 Power Supplies Power: 290 kW	
$ 842,276	$ 907,276	$ 65,000
Cables: $ 78,000	$163,260	$ 85,260

Table 43: Ring Quadrupoles Power Supplies (WBS 1.5.4.1.2).

July 99 Review	Present	Cost
Power Supplies	Power Supplies	Increase ($)
5 Power Supplies Power: 795 kW	5 Power Supplies Power: 1,200 kW	
$ 1,251,896	$ 1,441,896	$190,000
Cables: $ 136,240	$ 204,360	$ 68,120

This increase is for the omega configuration with the hybrid lattice. All changes, except for the RTBT, are required solely for the hybrid lattice ($ 1,377,462). The omega configuration requires 4 power supplies out of 7. Therefore, the omega portion of the RTBT increase is $ 200,789.

Hybrid Lattice increase: $ 1,377,462

Omega increase: $ 200,789

Total increase in Electrical Systems = $1,578,251

Table 44: Extraction Kicker Power Supplies (WBS 1.5.9.2).

July 99 Review	Present	Cost
Power Supplies	Power Supplies	Increase (K$)
8 units	14 units	
$ 1,483,196	$ 2,196,752	$ 713,556

Table 45: RTBT Power Supplies (WBS 1.5.10.2.1).

July 99 Review	Present	Cost
Power Supplies	Power Supplies	Increase (K$)
2 Dipoles, 14 Quads, Dump-2 Quads Power: 692 kW	2 Dipoles, 21 Quads, Dump-2 Quads Power: 1,133 kW	
$ 1,735,269	$ 2,023,269	$ 288,000
Cables: $ 194,620	$ 258,000	$ 63,380

7 Summary

With essentially no change of the ring circumference and ring dipole magnet dimension, the acceptance of the machine is increased by more than 50%, from 306 to 480 πmm·mr. Consequently, the collimation efficiency is increased from about 80% to 95%. The expected uncontrolled beam loss is reduced from 10^{-3} to 10^{-4} level. In addition, the long uninterrupted straight section provides flexibility for injection, collimation, and other arrangements [22].

The total unburdened system cost increase caused by the lattice change from the original all-FODO to the proposed hybrid structure, and the footprint layout change from the original alpha to the proposed omega configuration is about $ 2,447,470.

References

[1] *Spallation Neutron Source Design Manual*, June 1998.

[2] J. Wei, J. Beebe-Wang, M. Blaskiewicz, P. Cameron, G. Danby, C.J. Gardner, J. Jackson, Y.Y. Lee, H. Ludewig, N. Malitsky, D. Raparia, N. Tsoupas, W.T. Weng, S.Y. Zhang, "Beam-Based Design Optimization for the Spallation Neutron Source Ring" Proceedings of Particle Accelerator Conference, New York (1999) p. 3185.

[3] C. Gardner, Y. Y. Lee, N. Tsoupas, J. Wei, "An Alternative Lattice for the Spallation Neutron Source Accumulator Ring", Proceedings of Particle Accelerator Conference, New York (1999) p. 3182.

[4] T. Wangler, *RF Linear Accelerators*, Wiley & Sons, p. 285.

[5] T. Roser, private communications, 1999.

[6] M. Blaskiewicz, *Instabilities in the SNS*, PAC99 (1999) p. 1611.

[7] N. Catalan-Lasheras, et al, Workshop on beam scraping and collimation, 1999 (to be published).

[8] J. Wei, et al, Workshop on beam scraping and collimation, 1999 (to be published).

[9] N. Catalan-Lasheras, *Transverse and Longitudinal Beam Collimation in a High-Energy Proton Collider (LHC)*, Ph. D Thesis, Universidad de Zaragoza (1999).

[10] R. Witkover, et al, *Beam Instrumentation for the Spallation Neutron Source Ring*, PAC99 (1999) p. 2250.

[11] H. Ludewig, et al *Collimator Systems for the SNS Ring*, PAC99 (1999) p. 548.

[12] W.T. Weng, *SNS Accumulator Ring Design and Space Charge Considerations*, Workshop on Space Charge Physics in High Intensity Hadron Rings, AIP Conference Proceedings 448 (1998), p. 152.

[13] D. Raparia, private communications.

[14] J. Beebe-Wang, et al, *Transverse Phase Space Painting For SNS Accumulator Ring Injection*, PAC99 (1999) p. 1743.

[15] N. Malitsky, et al, *UAL-Based Simulation Environment for Spallation Neutron Source Ring*, PAC99 (1999) p. 2713.

[16] A. Fedotov, private communications.

[17] S. Machida, Nucl. Instrum. Methods, **A309** (1991) 43.

[18] ORBIT: written by J. Galambos et al.

[19] L. Schachinger, R. Talman, Part. Accel. **22**, 35 (1987).

[20] S.Y. Zhang, SNS Ring Technical Notes 33 (1997), 43 (1998), 61 (1999).

[21] S.Y. Zhang, *Secondary Electron Production at the SNS Storage Ring Collimator*, PAC99 (1999) p. 3297.

[22] J. Wei, et al, ICFA Newsletter No. 19 (April 1999), No. 20 (August 1999).